# Spectral- and Image-Based Metrics for Evaluating Cleaning Tests on Unvarnished Painted Surfaces

Jan Dariusz Cutajar * , Calin Constantin Steindal , Francesco Caruso , Edith Joseph , Tine Frøysaker

Posted Date: 11 July 2024

doi: 10.20944/preprints202407.0896.v1

Keywords: treatment evaluation; surface cleaning; soiling removal; agar gel; exposed grounds; unvarnished oil paints; Edvard Munch; spectral imaging

*Article*

# Spectral- and Image-Based Metrics for Evaluating Cleaning Tests on Unvarnished Painted Surfaces

**Jan Dariusz Cutajar [1,*], Calin Constantin Steindal [2], Francesco Caruso [3,4], Edith Joseph [5,6] and Tine Frøysaker [1]**

[1] Conservation Studies, University of Oslo, Norway; j.d.cutajar@iakh.uio.no; tine.froysaker@iakh.uio.no
[2] Cultural History Museum, University of Oslo, Norway; c.c.steindal@khm.uio.no
[3] Department of Art Technology, Swiss Institute for Art Research (SIK-ISEA), Zurich, Switzerland;
[4] Department of Analytical Chemistry, University of the Basque Country UPV/EHU, Vitoria-Gasteiz, Spain; francesco.caruso@ehu.eus
[5] Haute École Art Conservation-Restoration (HE-Arc CR), Haute École Spécialisée de Suisse Occidentale (HES-SO), Switzerland; edith.joseph@he-arc.ch
[6] Laboratory of Technologies for Heritage Materials, University of Neuchâtel, Switzerland;
* Correspondence: jd_c@outlook.com

**Abstract:** Despite advances in conservation-restoration treatments, most surface cleaning tests are subjectively evaluated. Scores according to qualitative criteria are employed to assess results, but these can vary by user and context. This paper presents a range of cleaning efficacy and homogeneity evaluation metrics for appraising cleaning trials, which minimise user bias by measuring quantifiable changes in the appearance and characteristic spectral properties of surfaces. The metrics are based on various imaging techniques (optical imaging by photography using visible light (VIS); spectral imaging in the visible-to-near-infrared (VNIR) and shortwave infrared (SWIR) ranges; chemical imaging by Fourier transform infrared (FTIR) spectral mapping in the mid-infrared (MIR) range; and scanning electron microscopy coupled with energy dispersive X-ray spectroscopy (SEM-EDX) element mapping). They are complemented by appearance measurements (glossimetry and colorimetry). As a case study showcasing the low-cost to high-end metrics, agar gel spray cleaning tests on exposed ground and unvarnished oil paint mock-ups are reported. The evaluation metrics indicated that spraying agar (prepared with citric acid in ammonium hydroxide) at a surface-tailored pH was as a safe candidate for efficacious and homogenous soiling removal on water-sensitive oil paint and protein-bound ground. Further research is required to identify a gel-based cleaning system for oil-bound grounds.

**Keywords:** treatment evaluation; surface cleaning; soiling removal; agar gel; exposed grounds; unvarnished oil paints; Edvard Munch; spectral imaging

## 1. Introduction

The conservation field is a rich and dynamic profession that has continuously drawn on its interdisciplinary nature to find appropriate remedial treatments for the challenges faced by its practitioners. The surface cleaning of decorative or painted surfaces is one such challenge that occupies conservators [1]. In this paper, *surface cleaning* will be referred to as the selective removal of deposited soiling upon painted surfaces. In turn, *soiling* is used to imply atmospheric particulate matter that deposits itself on heritage surfaces [2].

Besides traditional options, the repertoire of surface cleaning treatments available to conservators features adaptions from fields such as green chemistry [3], chemical engineering [4,5], and physics [6,7]. In recent years, notable improvements have been made with gel cleaning [8–24], which is the focus of this work.

Despite these advances, most of these cleaning treatments are still evaluated in a somewhat subjective manner. Scores according to pre-defined criteria are assigned to results of cleaning tests, following an ever more established practice within the profession [10,25,26]. This evaluation method

 doi:10.20944/preprints202407.0896.v1



is relatively easy to apply, and can also be visualised as star diagrams to better comprehend outcomes [10,27–31].

On one hand, this practice reflects the inherent nature of conservation practice. Every object requires to be treated differently based on its context [32–35]; and as specialised professionals, conservators will evaluate risk and success based on their training and experience. From a stakeholder/representative perspective, the perception of what makes a successful cleaning treatment is highly subjective too, and the concept of cleanliness can be said to be values- and/or community-based, as defined by contemporary conservation theory [36,37]. From this point of view, it is possible that a fully objective evaluation is perhaps not achievable, nor wholly desirable. On the other hand, subjective scorings, albeit assigned by trained and experienced eyes, are hard to reproduce, and are reliant upon many contextual factors that might skew the judgment of the assessor in question. From another perspective, the test surfaces often used in cleaning studies are not usually homogenous (due to their complex nature), and this might introduce further bias when attempting to weigh cleaning test outcomes.

Cleaning studies in conservation often use analogous mock-ups to mimic a material surface under investigation [38–43]. In this context, mock-ups are a critical tool for conservators to explore the behaviour of a heritage object with respect to a trialled treatment, whilst respecting the integrity of the object itself. The properties of the mock-ups can be selectively tuned for the treatment (or object) under study, and the mock-ups can be consumed/reproduced according to need, or even reused for future studies on the evaluation of a treatment over time [44,45].

Surface cleaning evaluations typically select a number of salient criteria upon which to assess the treatments under consideration. Generally, these may include cleaning assessment factors such as: soiling removal efficacy, homogeneity, selectivity (i.e. lack of pigment pick-up), surface disruption (e.g. by swelling, or foaming), residue deposition, and surface appearance (with respect to colour and gloss) amongst others [10,17,25,29,30]. An example of user-dependent criteria is given in Table 1.

**Table 1.** Example of cleaning criteria used in conservation studies [10,17,29,30].

| | Scoring Criteria | | | |
|---|---|---|---|---|
| **Score Rating** | **Cleaning Efficacy** | **Cleaning Homogeneity** | **Pigment Swelling** | **Selectivity (Pigment Loss)** |
| 1 | No effect | Uneven removal (<30%) | Extreme, visible swelling | Unacceptable loss |
| 2 | Little effect | Inconsistent removal (<50%) | Moderate, visible swelling | Notable loss |
| 3 | Moderate effect | Consistent removal (<80%) | Sensation of swelling, invisible | Microscopic loss |
| 4 | Effective removal | Complete removal (100%) | No swelling | No loss |

The above criteria are assessed visually as a function of change compared to a pre-determined surface condition by a conservator's trained eye, but this introduces user-bias into any evaluation, regardless of the expertise of the assessor. For this reason, the conservator's intuitive observations are often corroborated, with added empirical confidence, by measured analytical data. For example, optical and digital microscopy are usually employed to pick-up differences resulting from cleaning selectivity and surface disruption; colorimetry and glossimetry are used to measure changes in surface appearance, whereas SEM-EDX and FTIR imaging are used to monitor chemical changes in the surface, and residue deposition by treatments. Cleaning homogeneity and efficacy however remain based on estimates registered by the user.

Diagnostic imaging technologies (such as spectral imaging [46]) can provide opportunities to incorporate a high amount of empirical-based data that can act as a complementary aid for conservators in making more reliable, repeatable, and accurate assessments when assigning scores for novel treatment evaluations. Research efforts have already begun addressing this issue [45,47].

 doi:10.20944/preprints202407.0896.v1



To address and overcome user subjectivity, the methodology presented in this article offers the choice of non-contact and/or non-invasive image, appearance and spectral measurements, which conservators can avail of (according to access to instrumentation). The methodology takes advantage of the image-based outputs generated by various diagnostic imaging techniques, which can then be processed in freeware, such as FIJI (ImageJ) [48], to provide semi-quantitative percentage scores, thus offering a common platform for comparison. By juxtaposing these techniques together, this work thus aims to contribute towards offering a robust, rigorous, and comparable evaluation framework for documenting surfaces before and after soiling removal tests.

The evaluation metrics developed in this study were based on optical photography and microscopy, appearance-based measurements (colorimetry and glossimetry), and imaging spectroscopy (hyperspectral imaging (HSI), micro-Fourier-transform infrared (μFTIR) mapping, and energy dispersive X-ray spectroscopy (EDX) mapping). Notably, this paper applies established post-processing techniques in imaging spectroscopy to the evaluation of surface cleaning. Spectral unmixing algorithms were implemented to identify and map soiled and cleaned surfaces. These algorithms classify pure or mixed materials based on spectral similarity [49–51], either using user-defined, known references or libraries (e.g. semi-supervised unmixing by *PoissonNMF* [52]), or blindly classifying them into groups (e.g. unsupervised unmixing by *LUMoS* [53]). A chemometric method for normalised difference image (NDI) mapping [54–56] of soiled and cleaned surfaces is also reported. Using principal component analysis (PCA) [57], characteristic wavelengths in the shortwave-infrared (SWIR) were selected to represent and then map soiling on the surfaces under the study.

## 2. Materials and Methods

***Mock-ups.*** The case study presented in this article centres around mock-ups of Edvard Munch's (1865–1944) monumental unvarnished painting, *Kjemi* (1914–1916, Woll no. 1227), situated at the University of Oslo Aula (1911) in central Oslo. This painting forms part of a frieze of eleven monumental artworks (oil on canvas) under study within the CHANGE-ITN and Munch Aula Paintings (MAP) projects [57–59]. The mock-ups have been designed to study a new cleaning technique – agar gel spray – for unvarnished, water-sensitive painted surfaces [60] as a response to the heavy soiling history of the paintings within the Aula [44,61–66], as well as to test the applicability and suitability of the imaging techniques mentioned above for the documentation of the cleaning trials.

Figure 1 illustrates one protein-bound and one oil-bound exposed ground, and one unvarnished oil paint mock-up (5 cm × 5 cm), formulated based on material analyses of *Kjemi* [62,67]. An in-depth description of the mock-up surfaces is provided in Table 2. They were naturally and artificially aged to emulate the mechanical and water-sensitive properties of the Aula paintings. Artificial soiling was applied following a modified methodology adapted for the Aula context [68,69]. The artificial soiling recipe used is given in Table 3. The soiling comprised of insoluble macroscopic particulates (iron oxide, silica, kaolin), microscopic soot particles (carbon black), water-reactive solids (Portland cement, type I), hydrophilic organics (gelatine powder, soluble starch), and hydrophobic organics (olive oil, mineral oil), all dispersed in Shellsol D40 mineral spirits. The mock-ups were soiled across three cycles of accelerated ageing (Table 2). Excess soiling was applied to facilitate soiling detection. The mock-ups before treatment (BT) were therefore slightly more heavily soiled than is currently observed on the Aula paintings.

 doi:10.20944/preprints202407.0896.v1



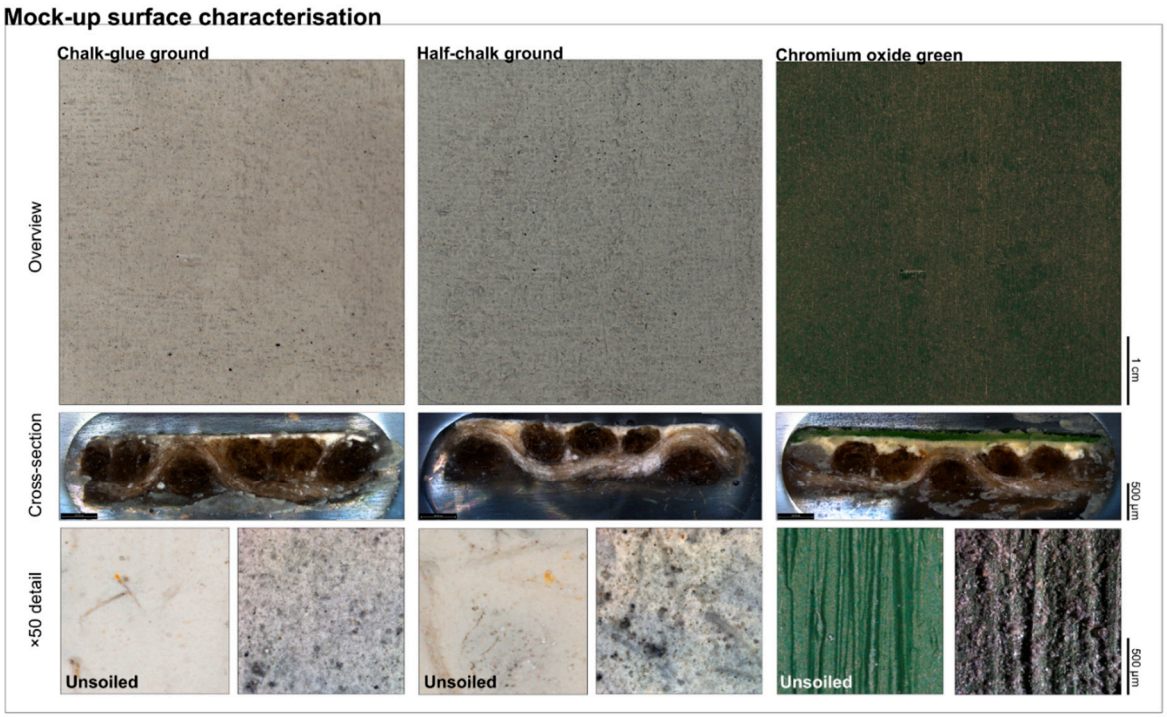


**Figure 1.** Overview (top row), cross-sections (central row), and magnified detail (bottom row) of the soiled mock-up surfaces (5 cm × 5 cm) cleaned during this study (unsoiled mock-ups are shown for comparison's purpose, indicating degree of soiling and differences in surface topography). The three mock-up classes included a chalk-glue ground, a half-chalk ground, and a chromium oxide green oil pain in linseed oil applied onto a half-chalk ground.

**Table 2.** Description and characterisation of mock-up surfaces prepared for the cleaning trials.

| Mock-Up | Stratigraphy | Application | Ageing and Soiling[a] | Surface Properties[b] |
|---|---|---|---|---|
| **Chalk-Glue Ground** | *Canvas*: washed linen, twill weave, stretched<br>*Size*: rabbit skin glue<br>*Ground*: chalk, in rabbit skin glue | Hog's hair brushes | 6 months ambient drying<br><br>3 weekly cycles of accelerated ageing: Memmert ICH110L chamber; light: 4 fluorescent lamps (6 500 K (D56), 500 W); irradiance: 70 $Wm^{-2}$; total energy: 169 330 $kJm^{-2}$; 40°C (CHT); and fluctuating RH (15–65%) | *Thickness*: 122.3 ±39.2 µm<br>*Water sensitivity*: 14 rolls<br>*Chalking*: ISO 2<br>*pH*: 6.5<br>*Conductivity*: 1 500 µS $cm^{-1}$ |
| **Composite Half-Chalk Ground** | *Canvas*: ibid.<br>*Size*: ibid.<br>*Ground*: chalk, zinc white, lead white in rabbit skin glue and boiled linseed oil emulsion | | | *Thickness*: 104.9 ±40.2 µm<br>*Water sensitivity*: 10 rolls<br>*Chalking*: ISO 3<br>*pH*: 6.4<br>*Conductivity*: 500 µS $cm^{-1}$ |
| **Chromium Oxide Green Oil Paint** | *Canvas*: ibid.<br>*Size*: ibid.<br>*Ground*: half-chalk ground<br>*Pigment-binder*: undiluted | | 3 spraying campaigns (2 for oil paint) of artificial soiling adapted for the Aula<br><br>*Soiling layer*: 27.1 ±2.4 µm<br>*Min particle size*: 0.095 µm | *Thickness*: 114.9 ±26.4 µm<br>*Water sensitivity*: 5 rolls<br>*Chalking*: ISO 1 |

 doi:10.20944/preprints202407.0896.v1



| | | | |
|---|---|---|---|
| chromium oxide green in linseed oil | *Max particle size*: | ≥10 μm | *pH*: 6.4<br>*Conductivity*: 530 μS cm$^{-1}$ |

*a*: applies to all mock-ups; *CHT* is chamber temperature, *RH* is relative humidity. *b*: *Thicknesses* are reported for topmost layer i.e. the cleaning surface; *water sensitivity* and *chalking* measurements from unsoiled mock-ups, according to Mills *et al.* [70], and UNI EN ISO 4628-6 [71] respectively; *pH* and *conductivity* measurements from soiled mock-ups, and are averages from triplicate measurements.

**Table 3.** List of components within the artificial soiling used in this study.

| Supplier | Material | Composition | Quantity | Dry Weight |
|---|---|---|---|---|
| | | | *g* or *mL* | % |
| Rublev | Lamp black (oil furnaces) | C | 0.62 | 1.00 |
| Kremer | Vine black (organic source) | C | 0.62 | 1.00 |
| | Burgundy ochre (fine) | $Fe_2O_3 \cdot H_2O$ | 1.45 | 2.34 |
| | Wheat starch powder | Polysaccharide $(C_6H_{10}O_5)_n$ | 10.00 | 16.14 |
| | Gelatin powder | Proteins and peptides | 10.00 | 16.14 |
| Merck | Sodium nitrate | $NaNO_3$ | 2.50 | 4.03 |
| | Kaolin | $Al_2Si_2O_5(OH)_4$ | 18.00 | 29.06 |
| | Portland cement (Type I) | $CaO \cdot SiO_2$ Fe, Al, MgO | 17.00 | 27.45 |
| | Silica, quartz | $SiO_2$ | 1.75 | 2.83 |
| | Mineral oil | Hydrocarbons | 5.0 | - |
| Filippo Berio | Olive oil | Mainly triacylglycerols | 2.5 | - |
| Kremer | Shellsol D40 | Hydrocarbons | 1000 | - |

***Agar spray and cleaning solutions.*** Agar spray is a novel form of agar gel cleaning, whereby the agar in sol state is subjected to atomisation within a heated paint applicator, allowing it to be applied as a homogenous and ultra-fine layer onto a surface within a very short time over large areas. The agar spray technique tested was developed by Giordano and Cremonesi [72,73], and an extensive characterisation of the new gel has been carried out by Giordano *et al.* [18]. Its properties make it an attractive candidate for the cleaning of soiled, textured painted surfaces, particularly those of a monumental scale such as those like Munch's Aula paintings.

Four aqueous cleaning solutions at various pH and conductivity values were selected as shown in Table 4. The selection was based on free-liquid trials (evaluated by naked eye and under optical microscope – assessments are available online as an externally hosted supplementary file).

**Table 4.** The four cleaning solutions selected from the free-liquid trials for use in the cleaning tests.

| Cleaning Solution | Concentration | Chalk-Glue Ground | Half-Chalk Ground | Chromium Oxide Green |
|---|---|---|---|---|
| Deionised water | - | pH 7.2, 20 μS cm$^{-1}$ | pH 7.2, 20 μS cm$^{-1}$ | pH 7.2, 20 μS cm$^{-1}$ |
| Adjusted water[a] (ammonium acetate) | Conductivity-related | pH 5.5, 1 500 μS cm$^{-1}$ | pH 5.5, 500 μS cm$^{-1}$ | pH 5.0, 500 μS cm$^{-1}$ |
| Chelator[b] (citric acid / sodium hydroxide) | 0.5% w/v (0.026M) CA in 10% w/v (2.5M) NaOH | pH 5.0, 4 240 μS cm$^{-1}$ | pH 4.5, 3 240 μS cm$^{-1}$ | pH 4.5, 3 240 μS cm$^{-1}$ |
| Chelator[b] (citric acid / ammonium hydroxide) | 0.5% w/v (0.026M) CA in 10% w/v (5.0M) $NH_4OH$ | pH 5.0, 5 320 μS cm$^{-1}$ | pH 4.5, 4 270 μS cm$^{-1}$ | pH 4.5, 4 270 μS cm$^{-1}$ |

 doi:10.20944/preprints202407.0896.v1



| | | | |
|---|---|---|---|
| Clearance[c] (ammonium acetate) | Conductivity-related | pH 6.5, 500 μS $cm^{-1}$ | pH 6.5, 500 μS $cm^{-1}$ pH 6.5, 500 μS $cm^{-1}$ |

*a*: buffer prepared from 1 mL 17.4M glacial acetic acid and adequate volume of 10% w/v (5.0M) ammonium hydroxide. *b*: citric acid diluted from a 2.5% w/v (0.13M) stock solution; conductivity of chelators could not be matched to surface properties as this would modify the chelator concentration. *c*: used after chelator; isotonic or hypertonic compared to mock-up surfaces at a pH where swelling is minimised.

Deionised water served as a control to investigate the effect of the gel application per se. Conductivity- and pH-adjusted waters were prepared for each type of mock-up class, following methodologies in the literature [68,74–76], and are referred to simply as *adjusted waters* throughout the remainder of the text. Monobasic and dibasic citrate chelating solutions (pH-adjusted with (i) NaOH; and (ii) $NH_4OH$, for comparative purposes, respectively) were selected to investigate chelating action, after being marked as promising for soiling removal in the Aula [17,77]. When using chelating solutions, a clearance solution (an appropriate adjusted water) was thereafter applied, as recommended by Stavroudis [78]. The pH and conductivity of used solutions were measured before use (deviating solutions were discarded and prepared freshly).

Agar gels were prepared with the different cleaning solutions, and applied in two ways: (i) as a direct spray [72,73], and (ii) as a pre-formed rigid film (prepared by spraying, as a milder modified form of cleaning). Clearance solutions were always applied as a pre-formed rigid gel (so that a double spray application did not interfere with interpretation of results). The gel was used at a concentration of 3% w/v, and sprayed evenly from a distance of 40 cm. The agar sol temperature prior to spraying was dependant on the room's and mock-up surfaces' temperature, and relative humidity. The experimental parameters measured during agar spray testing are given in Table S1. The gel was removed after two minutes, following recommendations by Giordano & Cremonesi [72,73].

***Treatment evaluation metrics***. A detailed description of the methodologies, including acquisition parameters, for each analytical technique is given in Appendix A. Table 5 below summarises the cleaning homogeneity and efficacy metrics, according to the range of the electromagnetic spectrum that they targeted, the multidimensional data types they employed, the concept through which they evaluated soiling removal, the equipment required to capture the data, and the post-processing steps needed to achieve results.

For each cleaning efficacy metric, a normalised difference was calculated according to Equation 1, where $x$ is a measured property before or after treatment (BT, or AT, respectively), so as to show the percentage return to an unsoiled control's surface property as a relative marker of cleaning success; the specific values used for each technique's metric are described in Table 6, further below.

$$\text{cleaning efficacy} = \frac{\boldsymbol{x}_{BT} - \boldsymbol{x}_{AT}}{\boldsymbol{x}_{BT}} \times 100 \quad (1)$$

All cleaning efficacy metrics were calculated in ImageJ, and then statistically treated, and plotted using the Microsoft Excel spreadsheet package. The results from the metrics were then fed into the scoring criteria listed below.

Because each painted surface has different cleaning requirements based on its inherent properties and condition [17], the evaluation process was adapted by weighting the scoring criteria to then recalculate a weighted average score out of 1.00. Based on discussions with the conservators who have treated and monitored the paintings over the past two decades, higher importance was given accordingly to cleaning efficacy and homogeneity (both 30% weighting), followed by selectivity (20% weighting) and then colour (15% weighting) and gloss integrity (5% weighting – gloss differences on the Aula paintings are only truly perceptible when standing directly underneath the paintings, which is not how the public typically views them). Calculation tables for the weighted scores are available online as an externally hosted supplementary file. Following what has become standard practice in cleaning studies in conservation [10,17,30,77], star diagrams were also used to

 doi:10.20944/preprints202407.0896.v1



illustrate the ideal cleaning candidate. The combination of weighted average scores with star diagrams permitted a thorough appraisal of the cleaning results.

**Table 5.** Summary of cleaning homogeneity and cleaning efficacy metrics described in this work.

| | Metric[a] | Range[b] | Data Type[c] | Concept | Equipment[d] | Post-Processing[e] |
|---|---|---|---|---|---|---|
| | ***Cleaning homogeneity*** | VNIR /SWIR | 2D spectral maps | Image homogeneity from grey-level co-occurrence matrix (GLCM) | DLSR camera HSI camera | Change image type to 8-bit depth for *GLCM Texture* plug-in in ImageJ |
| | ***Cleaning efficacy*** | | | | | |
| Image-based | *L*a*b** images | VIS | 2D RGB images | Thresholded pixels representing soiling | DLSR camera Mobile phone | Conversion to CIELAB space; image thresholding |
| Image-based | Histogram skewness | VIS | 2D RGB images | Histogram distribution asymmetry as function of darker soiling on lighter substrate | | Spreadsheet/statistical calculations |
| Appearance | Glossimetry | VIS | 1D point measurements | Perceived surface texture under direct light source | Glossmeter | Spreadsheet/statistical calculations |
| Appearance | Colorimetry (from HSI) | VNIR | 2D *L*a*b** images (from 3D datacube) | Colour difference, $\Delta E_{2000}$, before and after soiling removal | HSI camera | Conversion to CIELAB space; colorimetric and statistical calculations |
| Spectral-based | HSI: spectral unmixing | VNIR /SWIR | 3D datacube | Spectral reflectance similarity (compared to unsoiled areas, or soiling) | HSI camera | Spectral calibration; algorithm pre- and post-processing |
| Spectral-based | HSI: NDI mapping | SWIR | 2D normalised difference images | SWIR marker bands for soiling and surface | HSI camera | Spectral calibration; PCA; image processing |
| Spectral-based | FTIR mapping | MIR | 2D chemical maps | MIR spectra (or marker bands) for soiling | FTIR spectrometer | Atmospheric correction; correlation map profiles |
| Spectral-based | SEM-EDX mapping | (XR) | 2D chemical maps | Element signal for soiling | SEM | TruMap processing; element selection |

*a*: *L*a*b** (CIELAB (Commission internationale de l'éclairage) colourspace coordinates representing perceptual lightness and four colours of human vision, defined in 1976); HSI (hyperspectral imaging); FTIR (Fourier transform infrared); SEM-EDX (scanning electron microscopy with energy dispersive X-ray spectroscopy). *b*: VIS (visible light); VNIR (visible to near infrared); SWIR (shortwave infrared); MIR (mid-wave infrared); XR (X-rays; XRs are detected by spectrometers). *c*: 1D (one-dimensional); 2D (two-dimensional); 3D (three-dimensional). *d*: DLSR (digital single-lens reflex); *e*: PCA (principal component analysis).

 doi:10.20944/preprints202407.0896.v1



**Table 6.** List of measured properties, $x_{BT}$ and $x_{AT}$, for each metric inputted into the normalised difference equation used to calculate cleaning efficacy.

| | Cleaning Efficacy Metric | Value for $x_{BT}$ | Value for $x_{AT}$ |
|---|---|---|---|
| Image-based | *L*a*b** images | Number of black pixels before treatment (black pixels represent soiling) | Number of black pixels after treatment (black pixels represent soiling) |
| | Histogram skewness | Difference in skewness between unsoiled (CT) and soiled (BT) mock-up ($\Delta skewness_{CT,BT}$) | Difference in skewness between unsoiled (CT) and cleaned (AT) mock-up ($\Delta skewness_{CT,AT}$) |
| Appearance | Glossimetry | Difference in gloss between the unsoiled (CT) and soiled (BT) mock-up ($\Delta gloss_{CT,BT}$) | Difference in gloss between the unsoiled (CT) and cleaned (AT) mock-up ($\Delta gloss_{CT,AT}$) |
| | Colorimetry (from HSI) | CIE2000 colour difference between the unsoiled (CT) and soiled (BT) mock-up ($\Delta E_{2000(CT,BT)}$) | CIE2000 colour difference between the unsoiled (CT) and cleaned (AT) mock-up ($\Delta E_{2000(CT,AT)}$) |
| Spectral-based | HSI: spectral unmixing | Mean pixel value from 100 pixel x 100 pixel area taken from unsoiled (CT) mock-up, or soiling control (sCT), in unmixing map ($\bar{x}_{CT}$, or $\bar{x}_{sCT}$) | Mean pixel value from 100 pixel x 100 pixel area taken from cleaned (AT) mock-up, in unmixing map ($\bar{x}_{AT}$) |
| | HSI: NDI mapping | Mean pixel value from 100 pixel x 100 pixel area taken from unsoiled (CT) mock-up, or soiling control (sCT), in NDI map ($\bar{x}_{CT}$, or $\bar{x}_{sCT}$) | Mean pixel value from 100 pixel x 100 pixel area taken from cleaned (AT) mock-up, in NDI map ($\bar{x}_{AT}$) |
| | FTIR mapping | Number of white pixels before treatment (white pixels represent soiling) | Number of white pixels after treatment (white pixels represent soiling) |
| | SEM-EDX mapping | Number of element-rich areas as counted by *Analyse particles* function in ImageJ before cleaning | Number of element-rich areas as counted by *Analyse particles* function in ImageJ after cleaning |

## 3. Results and discussion

### *3.1. Metrics in Practice*

The metrics aimed to semi-quantitatively compare treatment results to aid in decision-making in a reproducible and shareable manner, and to complement professional observations made by eye. The image- and spectral-based metrics enhanced this process through their visual inputs and outputs, examples of which are illustrated in Figure 2 below. The appearance-based metrics were calculated from point measurements (Table 5), and therefore did not have any visual inputs nor outputs in terms of images or maps. It must be kept in mind that each metric measured a different property or component of the surfaces or soiling, and thus efficacy scores needed to be interpreted accordingly. Data plots for cleaning efficacy per metric are presented in Figures 3–10. Processed images from

 doi:10.20944/preprints202407.0896.v1



photography, microscopy, FTIR, and SEM, and data tables for all the efficacy plots discussed are available online as an externally hosted supplementary file.

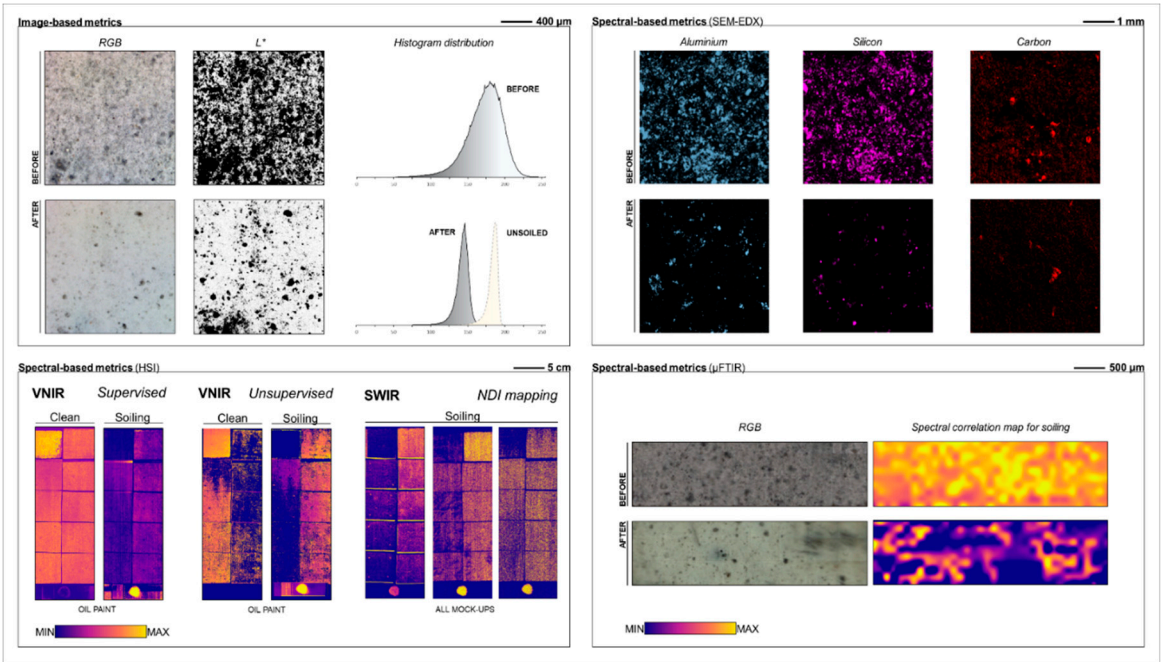


**Figure 2.** Examples of the visual outputs given by the image- and spectral-based metrics described • For the *image-based metrics*, figures are of the chalk-glue ground mock-ups cleaned with deionised water. The histogram distribution represents pixel values from 0 to 255 for the respective RGB images shown. • For the *HSI metrics*, only oil paint mock-ups are shown for spectral unmixing maps; all mock-up classes are shown for NDI maps (chalk-glue ground, half-chalk ground and oil paint from left to right). Each spectral map consists of a column of spray-cleaned mock-ups on the left, and a column of mock-ups cleaned by pre-formed rigid gel on the right (cleaning solutions on going from bottom to top: citric acid/$NH_4OH$, citric acid/NaOH, adjusted water, deionised water); unsoiled and soiled controls are found top left and right respectively. • For the *SEM-EDX* and *FTIR metric*, the example shown is for cleaning with citric acid/$NH_4OH$.

 doi:10.20944/preprints202407.0896.v1



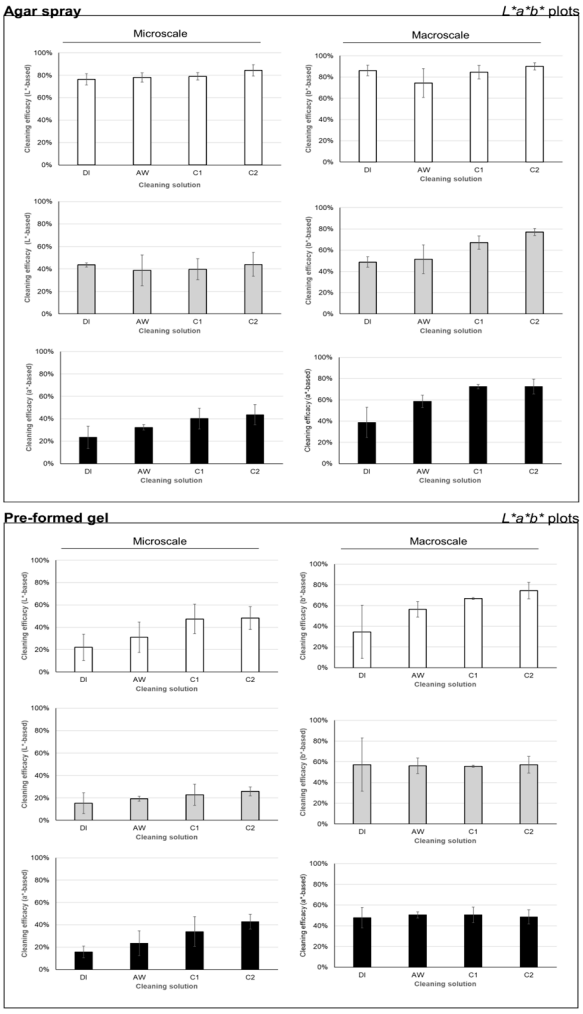


**Figure 3.** Cleaning efficacy plots using *L*a*b** images at micro- (*left*) and macroscale (*right*) for the spray-cleaned mock-ups (*top*) and the mock-ups cleaned by pre-formed gel (*bottom*) (keys: white – chalk-glue; grey – half-chalk; black – chromium oxide • (DI) deionised water; (AW) adjusted water; (C1) citric acid in NaOH solution; (C2) citric acid in $NH_4OH$ solution.

 doi:10.20944/preprints202407.0896.v1



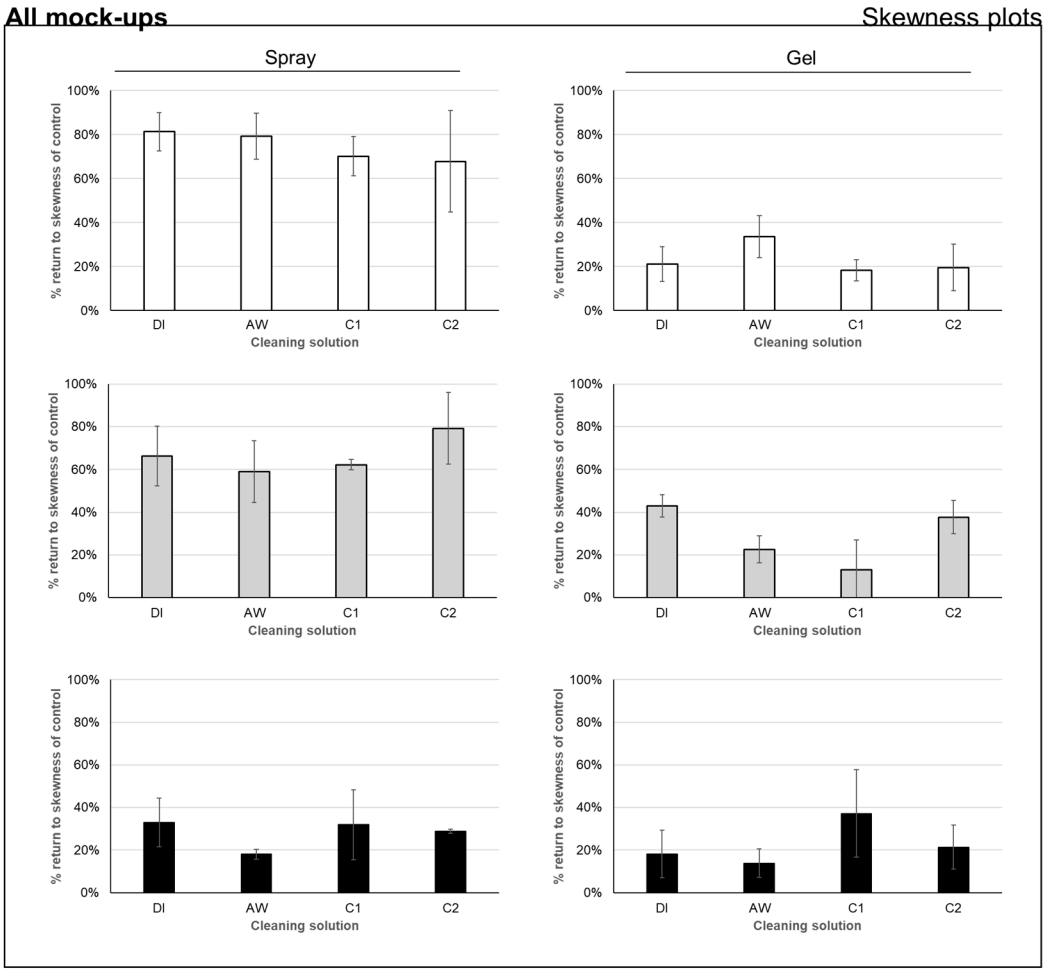


**Figure 4.** Cleaning efficacy plots based on skewness for the sprayed mock-ups (*left*) and the mock-ups treated by pre-formed gel (*right*) (keys: white – chalk-glue; grey – half-chalk; black – chromium oxide • (DI) deionised water; (AW) adjusted water; (C1) citric acid in NaOH solution; (C2) citric acid in $NH_4OH$ solution.

 doi:10.20944/preprints202407.0896.v1



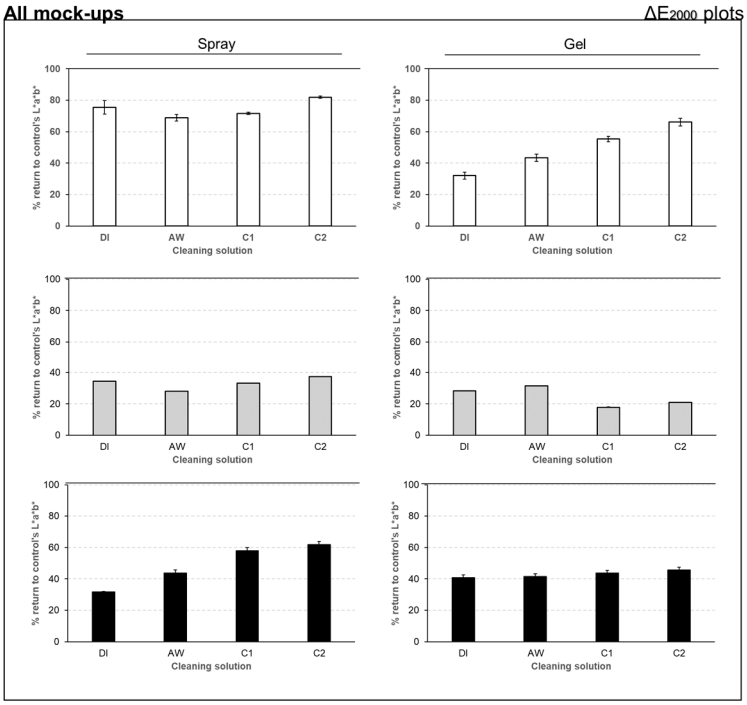


**Figure 5.** Cleaning efficacy plots based on $\Delta E_{2000}$ for the sprayed mock-ups (*left*) and the mock-ups treated by pre-formed gel (*right*) (keys: white – chalk-glue; grey – half-chalk; black – chromium oxide • (DI) deionised water; (AW) adjusted water; (C1) citric acid in NaOH solution; (C2) citric acid in $NH_4OH$ solution.

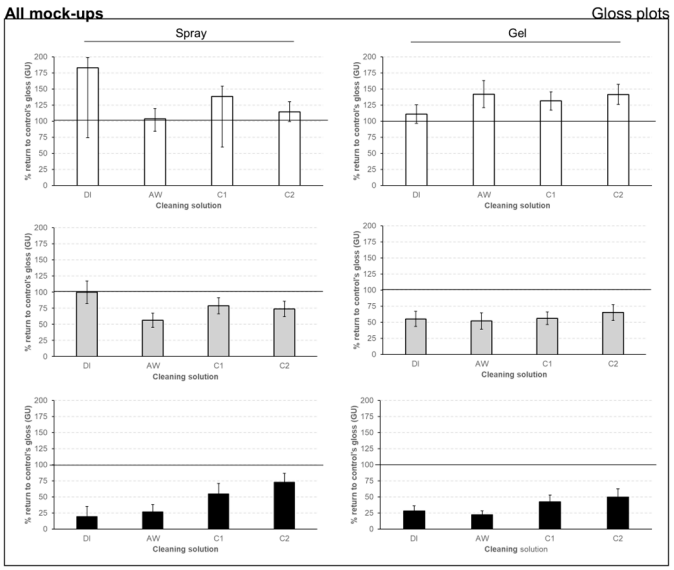


**Figure 6.** Cleaning efficacy plots based on glossimetry for the sprayed mock-ups (*left*) and the mock-ups treated by pre-formed gel (*right*) (keys: white – chalk-glue; grey – half-chalk; black – chromium oxide • (DI) deionised water; (AW) adjusted water; (C1) citric acid in NaOH solution; (C2) citric acid in $NH_4OH$ solution.

 doi:10.20944/preprints202407.0896.v1



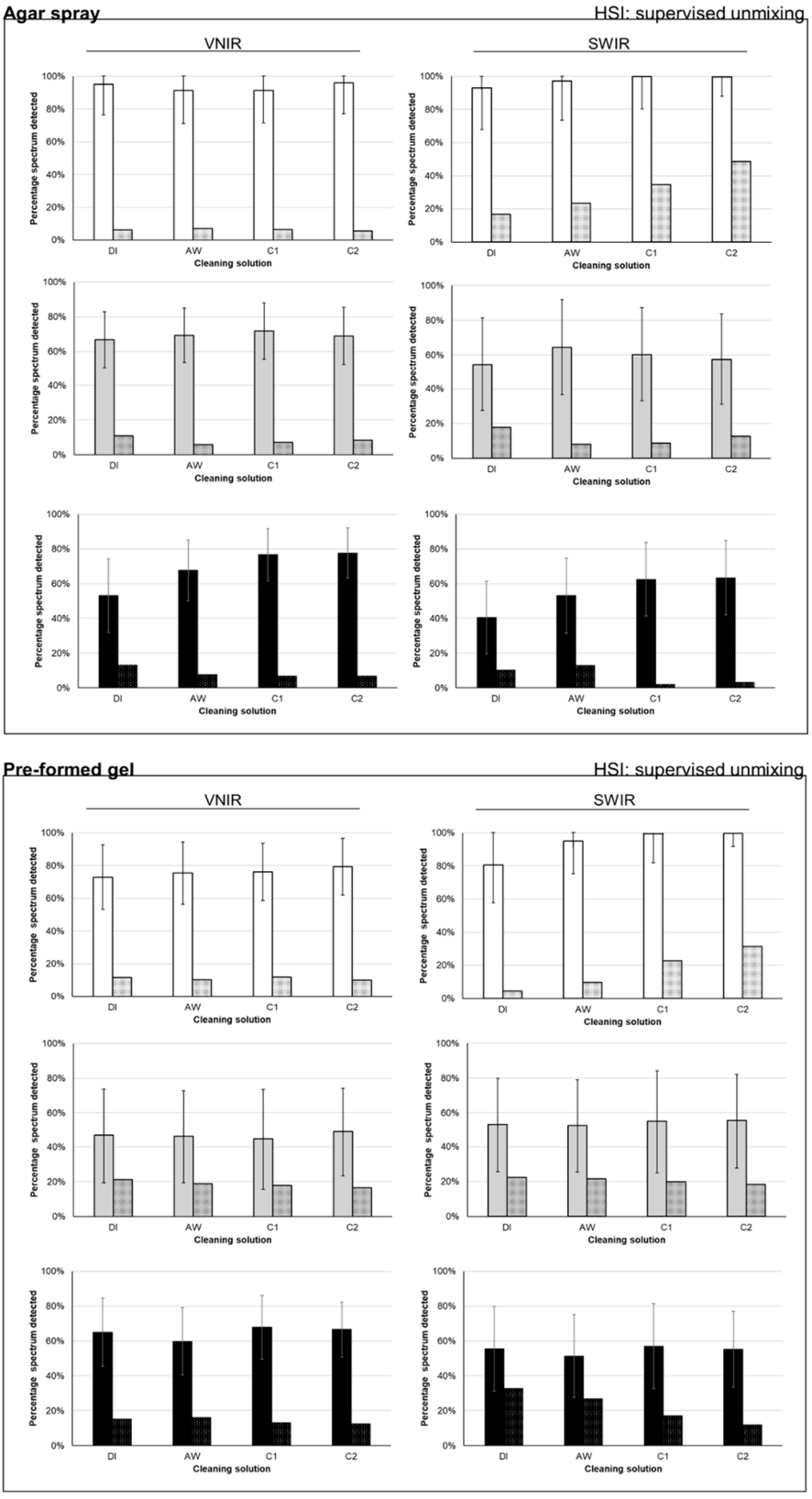


**Figure 7.** VNIR and SWIR metric plots as determined by the semi-supervised unmixing algorithm, based on clean (plain fill) and soiled (textured fill) reference spectra for spray-cleaned surfaces (*top*) and the pre-formed gel cleaning (*bottom*). Error plotted only for clean areas (RSD for soiled areas was above 1.00 in all cases) (keys: white – chalk-glue; grey – half-chalk; black – chromium oxide • (DI) deionised water; (AW) adjusted water; (C1) citric acid in NaOH solution; (C2) citric acid in $NH_4OH$ solution).

 doi:10.20944/preprints202407.0896.v1



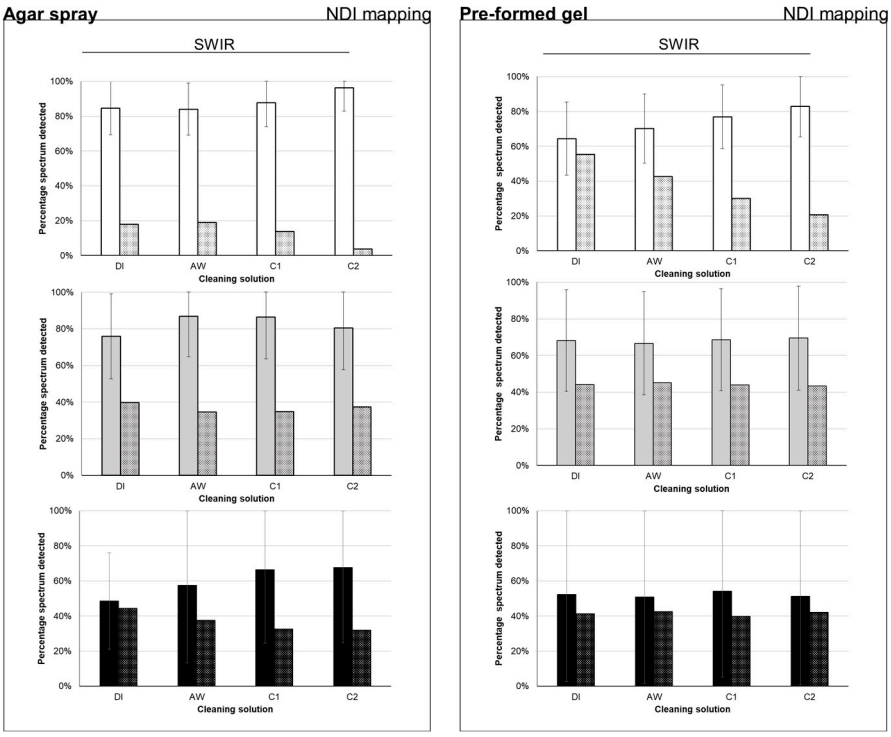


**Figure 8.** VNIR and SWIR metric plots as determined by the SWIR-NDI mapping, based on clean (plain fill) and soiled (textured fill) reference spectra for spray-cleaned surfaces (*left*) and the pre-formed gel cleaning (*right*). Error plotted only for clean areas (RSD for soiled areas was above 1.00 in all cases (keys: white – chalk-glue; grey – half-chalk; black – chromium oxide • (DI) deionised water; (AW) adjusted water; (C1) citric acid in NaOH solution; (C2) citric acid in $NH_4OH$ solution).

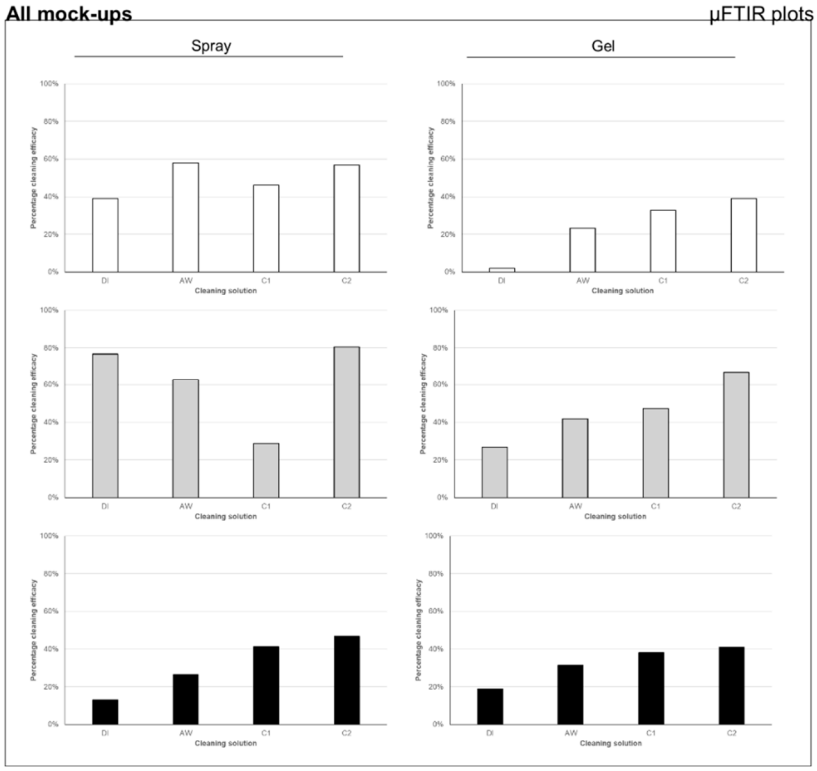


**Figure 9.** Cleaning efficacy plots for the sprayed gel (*left*) and plots for the pre-formed gel (*right*) based on the FTIR metric (keys: white – chalk-glue; grey – half-chalk; black – chromium oxide • (DI) deionised water; (AW) adjusted water; (C1) citric acid in NaOH solution; (C2) citric acid in $NH_4OH$ solution)..

 doi:10.20944/preprints202407.0896.v1



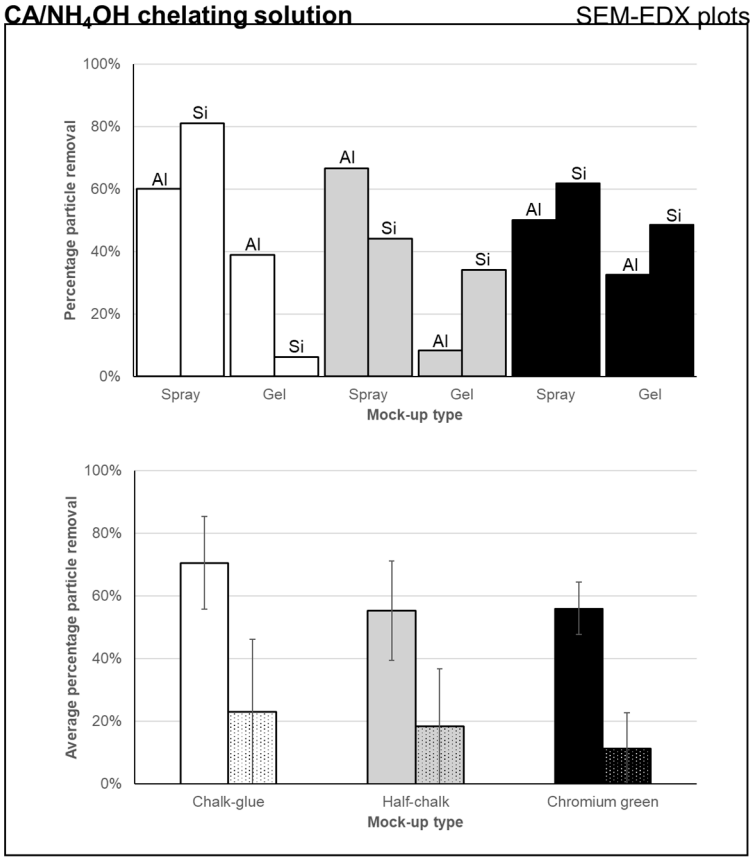


**Figure 10.** Cleaning efficacy plots for the SEM-EDX metric for particle removal by element (*top*) and average particle removal (*bottom*), using citric acid (CA) in an $NH_4OH$ solution (key: white – chalk-glue; grey – half-chalk; black – chromium oxide • plain fill – agar spray; textured fill – pre-formed gel).

3.1.1. Image-Based Metrics: L*a*b*

The images serving as input data for the image-based metrics were captured using the visible (VIS) range of the electromagnetic spectrum. The image-based metrics may be considered non-invasive, non-contact, as well as more accessible and low-cost, in that the only required equipment is a DSLR camera and/or a microscope. Having been converted from RGB to CIELAB colour space for this metric, the $L^*a^*b^*$ images offer insights into the perceptual lightness ($L^*$), and colours (as perceived by the human eye, $a^*$ and $b^*$) of the mock-up surfaces. The $L^*a^*b^*$ images thus serve as an extension to the conservator's eye. The metric in turn represents soiling distribution based on the pixel intensity values of the $L^*a^*b^*$ images. It should be kept in mind that the accentuation of soiling through pixel intensity depends upon the colours of the soiling and surface being investigated.

Cleaning efficacy results for images taken at microscale coincided better with visual observations than those taken at macroscale, which – although comparable in trend – tended to overestimate cleaning. This could have been possible due to the resolution and scale at which the images were captured, whereby macro-imaging might have not given a relatable representation of the distribution of soiling, based on the image processing method used. Furthermore, results for macro-photography were based on one mock-up (and not a set of triplicates, due to time restrictions), and thus did not cover the heterogeneity of soiling removal results. The remaining discussion therefore focuses on the microscale results.

Out of the possible $L^*$, $a^*$ and $b^*$ images generated for the mock-up surfaces imaged in this study, it was noticed that $b^*$ images gave better indications of the presence of soiling. This is since this channel did not pick up surface texture, which was prominent in $L^*$ images (this could be taken advantage of, nonetheless, to reveal crack propagation, for example). Resultantly, the $L^*$ channel was found to be better suited for smoother surfaces, and the $b^*$ channel for rougher, textured surfaces.

 doi:10.20944/preprints202407.0896.v1



Cleaning efficacy plots using *L*a*b** images are given in Figure 3. The spray application superseded the pre-formed gel in terms of cleaning efficacy. However, this was only marginally so for the oil paint mock-ups, indicating that application method of the gel did not influence soiling removal for this mock-ups class, perhaps as result of the physicochemical means of soiling-to-surface binding.

For the pre-formed gel application, there was a notable increase in performance of soiling removal for the citrate/$NH_4OH$ solution, compared to other cleaning solutions. This trend was less apparent with respect to the spray application, but the metric indicated that the same chelating solution removed the most soiling, nonetheless. Overall, the chalk-glue ground was cleaned almost twice as much as the other mock-up types, potentially reflecting differences in soiling-surface interaction.

Based on these observations, this metric offered reasonable representations of soiling removal efficacy, although it must be noted that the thresholding of the *L*a*b** images can be time-consuming and user-dependant.

### 3.1.2. Image-Based Metrics: Skewness

The use of statistical moments (describing the shape of a histogram distribution) as indicators of cleaning efficacy is based on the concept that, as darker contaminants are removed from lighter substrates, the pixel values of the respective BT and AT images reflect this change accordingly, and thus an image's histogram distribution can reflect the change taking place during cleaning. When considering a distribution's skewness in a cleaning context, a larger fraction of darker pixels (i.e. darker contaminants from soiling) will skew an image's histogram leftwards (negative skewness), whereas a larger fraction of lighter pixels (i.e. cleaner, lighter surfaces) skews the histogram rightwards (positive skewness).

The skewness metric has been successfully applied to stone cleaning [79] and paper cleaning [45], and hence was investigated for its promising application to the exposed grounds and unvarnished oil paint under study, as a fast and reliable measure. This metric was applied to the RGB micrographs, but could equally be applied to RGB macroscale photographs, as in the work by Charola *et al.* [79].

All three methods for calculating skewness were investigated during trials: they differed in how and which statistical descriptors were inputted for calculation [80]. Consequently, calculations indicated that Pearson's moment coefficient best described the skewness of histogram distributions in this case, in contrast to the cited studies that used Pearson's first and second coefficients. The selection was based on the coefficient that described the datasets best. Whereas only skewness was measured in this study, other moments such as the mean and kurtosis (flatness) of the distributions could have been additionally used to monitor changes after cleaning [79], and require further investigation for application onto unvarnished painted surfaces.

Histogram distributions of the micrographs are available online as an externally hosted supplementary file. The unsoiled mock-ups had a negative skewness (probably due to stray, darker pixels relating to canvas details, surface texture and irregularities), with a narrow distribution spread across lighter pixel values (Figure 2). The soiled ground mock-ups were characterised by less skewed and broader distributions across the centre of the plot, which narrowed and shifted towards lighter pixel values with an increased negative skewness (closer to the control's) after cleaning (Figure 2). The soiled paint mock-ups contrarily featured positively skewed distributions centred over darker pixel values (attributed to the soiling, and chromatic changes during ageing when compared to the control), which became more positively skewed as a higher percentage of lighter pixel values were present after removal of darker soiling (the distributions remained, however, centred over darker pixels due to the inherently darker substrate).

Cleaning efficacy plots based on skewness are given in Figure 4. The efficacy plots generated through the skewness metric indicated that the agar spray application resulted in better soiling removal than the pre-formed gel, which matched visual observations. The poorer performance of both gel applications when applied to the oil paint (as opposed to the grounds) was notable, and

 doi:10.20944/preprints202407.0896.v1



might be explained by the fact that considerable chemically imbibed soiling was observed microscopically after cleaning.

When comparing the cleaning of both grounds, the metric seems to overestimate the efficacy for the half-chalk ground, which looked effectively more soiled than its chalk-glue counterpart on the basis of visual observations. Whilst the chelating solutions removed most soiling on the half-chalk ground and the oil paint, the adjusted water gave better results for the chalk-glue ground. In the latter case, the uncovering (or formation) of micro-cracks and other surface details by the chelating solutions may have resulted in an increase in darker pixels, which according to this metric will translate into less efficacious cleaning.

### 3.1.3. Appearance-Based Metrics: Colour and Gloss

The management of changes to the colour and gloss of an object's surface is typically one of the fundamental priorities of the conservator during treatment [81–84], so as not to misrepresent the aesthetic value of the piece and detract from its creator's intent [85]. These metrics are not novel in themselves, but rather complemented the scoring criteria selected to evaluate the agar spray treatment.

Hyperspectral data was used for the colorimetry metric. Thus, one single data acquisition simultaneously allowed for both the measurement of colour change as a result of soiling removal, and the application of the spectral-based metrics (introduced after this section). This saved on time, and rendered measuring colorimetric data a completely non-contact process (colorimetric measurements are usually taken by placing a colorimeter upon the surface of an object).

The cleaning efficacy plots based on the measured changes in colour ($\Delta E_{2000}$) are given in Figure 5. The plots indicated that the cleaning solutions applied by spray guaranteed a better return to the colour of the unsoiled control than the pre-sprayed counterpart. The chelating solutions once again afforded the most efficacious soiling removal with respect to colour change. However, the half-chalk ground fared most poorly of all mock-up classes, irrespective of cleaning solution. This was likely due to soiling-surface interactions, whereby remaining imbibed soiling detracted from the full appreciation of the cream- coloured ground. The pre-formed gel, however, did offer an effective option for promoting return to the surfaces' original colours, especially with the citrate/$NH_4OH$ solution.

For glossimetry, the metric returns the difference with respect to the control's gloss, or if the change registered goes beyond that gloss measurement, the percentage of excess deviation beyond the control's gloss. Cleaning efficacy plots based on glossimetry are given in Figure 6.

For the chalk-glue ground, both the spray and pre-formed gel resulted in glossier surfaces after treatment. Given the large extent of matte areas of exposed chalk-glue ground in the Aula, this is a consideration worth addressing. Keeping in mind the variability of the gloss measurements, the most viable options for the cleaning of this ground were the adjusted water, followed by the citrate/$NH_4OH$ solution (both applied via spray).

With respect to the half-chalk ground and the chromium oxide oil paint, spraying the agar appeared to promote an improved return to the original gloss, with the chelating solutions delivering the best results.

### 3.1.4. Spectral-Based Metrics: HSI

The HSI metrics illustrated the degree of soiling removal across the VNIR and SWIR ranges, thus assessing soiling removal efficacy based on the physical properties and molecular composition of the cleaned surfaces, or soiling. An example of soiling mapping is shown in Figure 2 (bottom left). All spectral maps generated from HSI post-processing are provided in Figures S1–S16. One metric used spectral unmixing algorithms to map soiling removal, whereas the other one was based on the chemometric technique of normalised difference image (NDI) mapping. As a result of HSI setup and mock-up dimensions, the major advantage of these metrics was that they permitted the simultaneous mapping of soiling across the entire surface of many mock-ups using a single acquisition. The HSI method can therefore be considered as a non-contact, and relatively fast means of visual assessment.

 doi:10.20944/preprints202407.0896.v1



Between the two spectral unmixing algorithms tested, the semi-supervised one gave the most reliable results, whereas the unsupervised algorithm suffered from some issues. These issues are presented and discussed in Appendix B. The remainder of the discussion here focuses on the semi-supervised algorithm.

The VNIR and SWIR spectral unmixing maps using the spectrum of the unsoiled reference as an endmember demonstrated that (i) all the chalk-glue ground mock-ups were cleaned to a high degree with the spray, (ii) all half-chalk ground mock-ups were cleaned to a lesser degree, and (iii) that the oil paint mock-ups gradually became cleaner on going from deionised water to adjusted water to chelating solutions. The milder cleaning effect of the pre-formed gel was also mapped.

The converse relationship between spectral maps for cleaned areas (based on the unsoiled control's spectrum as an endmember) and for soiled areas (based on the soiled control's spectrum as an endmember) illustrated that soiling removal can be mapped using either reference spectrum. In the VNIR range, maps using the soiling's spectrum as an endmember reflected the contrary of the cleaned maps, i.e. they showed in a complementary fashion the presence of soiled areas, instead of cleaned ones.

In the SWIR range, indirect molecular markers of the soiling were detected [57]. These markers lend great use since soiling may not always be visible, e.g. where surface contrast is poor (dark soiling on dark surfaces), or where soiling/degradation products are not necessarily visible to the naked eye. However, in the case of the SWIR maps, false positives were detected in all cases, with soiling apparently present on unsoiled controls. In the case of the chalk-glue ground, the cleaner mock-ups were shown as the most soiled. This may have been due to the unmixing algorithm confounding spectral bands common to the soiling and the mock-up surfaces (related to the binder, for example).

For this reason, the semi-supervised HSI metric was best assessed using VNIR map pixel values (when using maps based on the unsoiled reference spectrum, however, SWIR map pixel values gave results that closely matched their VNIR counterpart). Cleaning efficacy plots based on the semi-supervised algorithm are given in Figure 7. The VNIR plots showed that using the agar spray with the chelating solutions, (i) over 90% of soiling was removed from the chalk-glue ground mock-ups, (ii) roughly 70% of soiling was removed from the half-chalk ground mock-ups, and (iii) about 80% of soiling removal was achieved for the oil paint mock-ups. The figures for the pre-formed gel were comparably lower, with the chelating solutions performing marginally better for all mock-ups.

In contrast to the spectral unmixing metric, the soiling removal maps generated through the NDI method provided more reliability with respect to detecting the presence or absence of soiling upon surfaces. This is due to the use of specific marker bands, which were significantly indicative of the materials being mapped (*cf.* Figure A1). However, this method required more expertise and time to achieve reliable results, as it implied carrying out multivariate statistical analysis on the datacubes collected. The semi-supervised unmixing algorithm is thus preferrable where advanced statistical expertise (or time) is lacking.

Cleaning efficacy plots based on SWIR-NDI maps are given in Figure 8. The NDI soiling removal efficacy plots matched with the observations made by eye, for both spray and pre-formed gel applications. The latter was marked as being less effective compared to its spray counterpart, irrespective of cleaning solution (except in the case of the chalk-glue ground). When the agar was sprayed, the maps and plots indicated the chelating solutions removed most soiling, particularly for the oil paint (in the case of the half-chalk ground, performance was also matched by the adjusted water).

The processed SWIR data from the NDI maps was further used to calculate a cleaning homogeneity score. As a complement to the cleaning efficacy metrics, this score was developed with the intention of empirically evaluating the degree of similar cleaning, i.e. homogeneity, achieved across the mock-ups' surfaces. In digital image analysis, a parameter for measuring image homogeneity was described by Haralick *et al.* [86,87], for which a plug-in in ImageJ was developed by Cabrera [88]. This parameter is calculated from what is known as the *grey level co-occurrence matrix* (GLCM) of an image [89,90]. Since the pixels in the images of the soiling maps can represent soiling

 doi:10.20944/preprints202407.0896.v1



spread, the homogeneity parameter (also known as the *inverse difference moment*) from the GLCM was deemed an appropriate measure of calculation.

#### 3.1.5. Spectral-Based Metrics: FTIR

The FTIR metric enabled an in-depth look at the cleaned surfaces at the microscale, providing imaging and spectral information from the mid-infrared (MIR) range. Cleaning efficacy plots based on μFTIR maps are given in Figure 9. The FTIR soiling maps illustrate the distribution of points where the soiling spectrum was detected. As a result, only those points where no soiling bands were detected were considered as clean, and this binary separation between soiled and cleaned could explain the lower percentages reported across the board when compared to HSI.

For the spray application, soiling removal was more effectively carried out on the exposed grounds than on the oil paint. This might reflect the nature of the soiling, which may have been more physically imbedded than chemically imbibed for the grounds. In terms of cleaning solution, the citrate/$NH_4OH$ solution outperformed the other options, both for spray and gel. Whereas this improved efficacy gradually increased across different solutions with the pre-formed gel, less certain trends were reported for the spray.

#### 3.1.6. Spectral-Based Metrics: SEM-EDX

A cleaning efficacy metric was developed using element mapping (SEM-EDX). One indirect, empirical observation that indicated the cleanliness of surfaces was the increased surface charging on AT surfaces during measurements, as there was less (carbon-containing) particulate matter to dissipate the electrons. Although the acquisition of data was slower than for HSI, the post-processing was relatively straightforward. This means that if chemical markers for soiling can be found, as with Al and Si in this case (due to their relative abundance within the artificial soiling), then the method could be a viable technique for monitoring cleaning. However, compared to all the other techniques discussed prior, the higher cost and significant operational expertise required to run such analyses, need to be borne in mind. For this very reason, only mock-up surfaces cleaned with citric acid in $NH_4OH$ were mapped.

The element maps collected indicated that soiling removal was most efficacious from the chalk-glue ground surfaces, whereas about half as much soiling was removed from the half-chalk and oil paint. Cleaning efficacy plots based on SEM-EDX element maps for Al and Si are given in Figure 10. As a result of the nature of data collected for this metric, it was also possible to calculate that the agar spray removed on average three times more soiling than its pre-formed gel counterpart.

### *3.2. Evaluating Soiling Removal Scores Using the Metrics*

The constellation of cleaning efficacy metrics, together with the cleaning homogeneity score, permitted a well-rounded assessment of the agar spray cleaning tests on the Aula mock-ups. Table 7 below shows an example of how the metrics compared to each other, and contributed towards the scoring criteria for the spray tests. The collection of scoring tables for all mock-ups are available online as an externally hosted supplementary file. The resulting star diagrams are presented in Figure 11 (overleaf).

**Table 7.** Breakdown of results from the cleaning efficacy metrics (*top*), and overall scoring criteria (*bottom*) for the chalk-glue ground mock-up triplicates sprayed by agar gel. The coloured values indicate the measured values used to calculate mean values (in bold): the red values refer to image-based cleaning efficacy scores, whereas as the blue values refer to spectral-based cleaning efficacy scores. The cleaning efficacy score in bold violet in the bottom table is the mean of the bold red and blue mean values.

| *Cleaning Efficacy Metrics* | | *Mean Values* |
|---|---|---|
| **Image-Based** | **Spectral-Based** | |

 doi:10.20944/preprints202407.0896.v1



| Cleaning Solution | *L*a*b** | Skewness | Supervised (VNIR) | NDI (SWIR) | FTIR (MIR) | Image-Based | Spectral-Based |
|---|---|---|---|---|---|---|---|
| Deionised water | 0.76 | 0.81 | 0.95 | 0.85 | 0.39 | **0.79** | **0.73** |
| Adjusted water | 0.78 | 0.79 | 0.91 | 0.84 | 0.58 | **0.79** | **0.78** |
| Chelator (NaOH) | 0.79 | 0.70 | 0.91 | 0.88 | 0.46 | **0.75** | **0.75** |
| Chelator ($NH_4OH$) | 0.84 | 0.68 | 0.96 | 0.96 | 0.57 | **0.76** | **0.80** |

*Scoring criteria*

| Cleaning Solution | Cleaning Efficacy[a] | Cleaning Homogeneity[b] | Colour Integrity[c] | Gloss Integrity[c] | Selectivity[d] | Residue Absence[d] |
|---|---|---|---|---|---|---|
| Deionised water | **0.76** | 0.23 | 0.75 | 0.17 | 1.00 | 1.00 |
| Adjusted water | **0.78** | 0.22 | 0.69 | 0.64 | 1.00 | 1.00 |
| Chelator (NaOH) | **0.75** | 0.33 | 0.72 | 0.62 | 0.60 | 1.00 |
| Chelator ($NH_4OH$) | **0.78** | 0.57 | 0.82 | 0.86 | 0.80 | 1.00 |

*a*: from metrics in upper table; *b*: from GLCM; *c*: from appearance-based metrics; *d*: user-defined (Appendix A).

For the chalk-glue ground and the chromium oxide green oil paint, the star diagrams indicate that the citrate/$NH_4OH$ solution (having the largest pentagon) satisfied most cleaning criteria. The solution's improved cleaning action was more evident when applied via spray than as a pre-formed gel, an observation that was already noticeable when evaluating the metrics and weighing in the results by eye. When applied as a pre-formed gel, the difference in base for the chelating agent was shown to be minimal, in fact for the oil paint, the citrate/NaOH solution was just about better.

The citrate/NaOH solution also seems to perform better for spray application on the half-chalk ground – however, it is interesting to note that at first glance the largest pentagons are those associated with deionised water, and therefore the action of the gel itself. Two implications follow from this: the first is methodological, in that combining the star diagrams with weighted scores is beneficial for dispelling vagueness that might result from having many polygons on one star diagram. For example, in the case of the star diagram for the pre-formed gel on the chalk-glue ground, the pentagons for deionised water and for the citrate/$NH_4OH$ solution may almost seem similar in size – the weighted score however indicates the chelating agent's improved performance, reflected also in the more central spread of its pentagram towards the prioritised criteria. The second consequence is more application-based. The cleaning solutions tested for the half-chalk ground were not as effective as expected, and the fact that the control solution of deionised water performed very similarly, or even better, than other tailored solutions implies that more experimentation is required to find a better candidate for cleaning.

The star diagrams also illustrate that cleaning homogeneity was best achieved when spraying the agar directly onto the surface, and the highest homogeneity was delivered by the chelator solutions.

 doi:10.20944/preprints202407.0896.v1



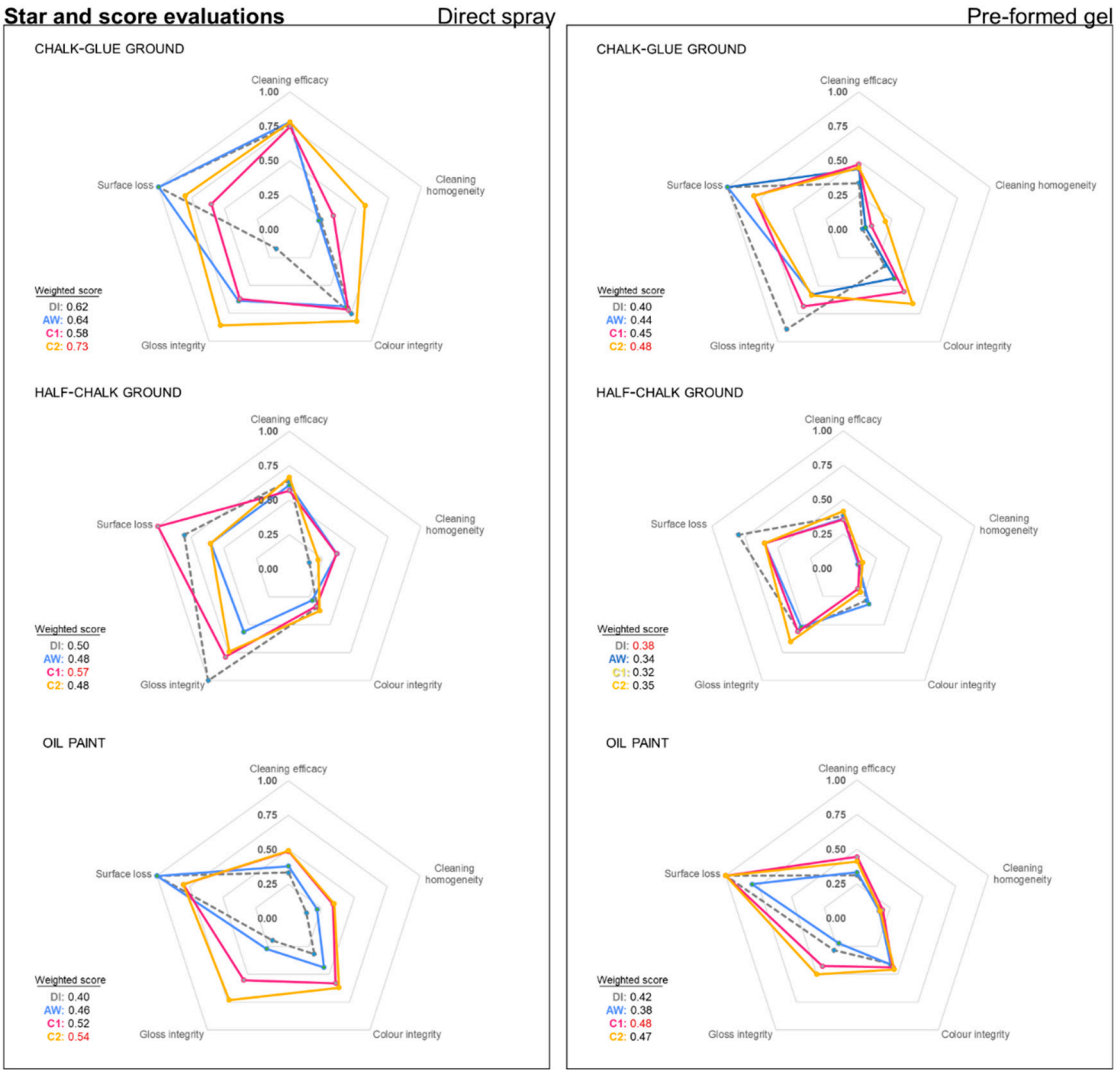


**Figure 11.** The star diagrams and weighted score evaluations of the agar cleaning trials (grey, dotted – deionised water (DI); blue – adjusted water (AW); crimson – citric acid in NaOH solution (C1); amber – citric acid in $NH_4OH$ solution (C2)). The weighted score highlighted in red indicates the highest score.

In the end, the suggestions for more empirical-based evaluations in this paper, combined with the tools that have developed within the profession, can further improve decision-making for conservators when planning a treatment, including at monumental scale, such as in the Aula. The presentation of results in this format makes it easier to document cleaning trials, and can aid in discussion with other heritage or museum colleagues, such as curators, private owners, art historians, archaeologists, and so forth.

## 4. Conclusions

The multidisciplinary approaches presented expand on the means currently available to conservators for empirically evaluating cleaning tests within a treatment context. By measuring changes in the appearance and spectrally characteristic properties of the surfaces being cleaned, the metrics introduced aim to minimise on user bias. They offer a toolkit of methods, which are relatively straightforward to execute, and can promote the quality of documentation, as well as the cross-dissemination of results in the literature.

Two major forms of cleaning efficacy have been defined, namely, spectral- and image-based efficacies. The spectral metrics are rooted in data collectable from a broad section of the electromagnetic spectrum, providing insights on different element, colorimetric, and molecular

 doi:10.20944/preprints202407.0896.v1



features. Where access to specialised equipment for measuring spectral-based efficacy is limited (due to budget, time restraints, etc.), the image-based efficacy metrics offer a low-cost, reliable and effective alternative to surface evaluation. These scores, calculated using image processing methods, tend to be lower than spectral-based scores, and thus mitigate against over-estimating cleaning.

An empirical means of calculating cleaning homogeneity based on digital image analysis was also used in evaluating the cleaning tests, together with a simplified, non-contact means of measuring colour change using hyperspectral imaging. Moreover, the representativeness of each metric's outputs was assessed by comparison to visual observations made by conservators. The newly proposed metrics were integrated as weighted scores with the star diagram evaluation system already established in conservation practice. Such an integration permitted a nuanced interpretation of cleaning tests by agar spray cleaning, comparing it to its pre-formed gel counterpart.

For exposed chalk-glue grounds and chromium oxide oil paint – two water-sensitive materials used by Edvard Munch in the Aula – spraying agar prepared with citric acid in ammonium hydroxide at a surface-tailored pH was evaluated as potentially the best candidate to date for efficacious and homogenous soiling removal. Notably, the pre-formed agar can be used to deliver milder, albeit slightly less effective, cleaning of fragile areas. It remains to be seen which cleaning solution is more appropriate for the half-chalk ground, and progress can be made once the nature of soiling-surface interactions on this type of ground is further elucidated.

It must also be considered that the Aula paintings themselves might be more fragile, and more water sensitive, than the mock-ups used in this study, and therefore further testing upon the artworks themselves is certainly required. This applies especially to areas that have poor surface adhesion, or have been previously consolidated [17]. For all the water-sensitive surfaces considered in this study, the effect of agar gel cleaning on other chemical forms of degradation, such as metal soap formation, has not been studied and should be considered. This is especially since developments in reflectance imaging spectroscopy for the detection of degradation products are picking up momentum [91–95].

Finally, the evaluation metrics themselves will benefit from further testing in other case studies to ensure their usefulness and applicability in the conservation profession. Further developments in the spectral imaging technologies and post-processing methods reported are certain to ameliorate the representativity of the metrics, which can be further tailored according to need in collaboration with conservators, conservation scientists and imaging scientists.

**Supplementary Materials:** The following supporting information can be downloaded at the website of this paper posted on Preprints.org, *Figure S1*: Legend to interpreting the spectral unmixing maps presented in this work; *Figure S2*: Spectral maps by supervised unmixing for the chalk-glue ground in the VNIR range; *Figure S3*: Spectral maps by supervised unmixing for the chalk-glue ground in the SWIR range; *Figure S4*: Spectral maps by supervised unmixing for the half-chalk ground in the VNIR range; *Figure S5*: Spectral maps by supervised unmixing for the half-chalk ground in the SWIR range; *Figure S6*: Spectral maps by supervised unmixing for the chromium oxide oil paint in the VNIR range; *Figure S7*: Spectral maps by supervised unmixing for the chromium oxide oil paint in the SWIR range; *Figure S8*: Spectral maps by unsupervised unmixing for the chalk-glue ground in the VNIR range; *Figure S9*: Spectral maps by unsupervised unmixing for the chalk-glue ground in the SWIR range; *Figure S10*: Spectral maps by unsupervised unmixing for the half-chalk ground in the VNIR range; *Figure S11*: Spectral maps by unsupervised unmixing for the half-chalk ground in the SWIR range; *Figure S12*: Spectral maps by unsupervised unmixing for the chromium oxide oil paint in the VNIR range; *Figure S13*: Spectral maps by unsupervised unmixing for the chromium oxide oil paint in the SWIR range; *Figure S14*: Normalised difference image map for the chalk-glue ground in the SWIR range; *Figure S15*: Normalised difference image map for the half-chalk ground in the SWIR range; *Figure S16*: Normalised difference image map for the chromium oxide oil paint in the SWIR range; *Table S1*: Environmental parameters measured during agar spray tests.

**Author Contributions:** Conceptualisation, J.D.C. and T.F.; methodology, J.D.C., C.C.S. and E.J.; software, C.C.S.; validation, J.D.C., C.C.S., E.J., F.C. and T.F.; formal analysis, J.D.C. and F.C.; investigation, J.D.C. and C.C.S.; resources, E.J., and T.F.; data curation, J.D.C.; writing—original draft preparation, J.D.C.; writing—review and editing, C.C.S, F.C., E.J., and T.F.; visualization, J.D.C. and F.C.; supervision, E.J. and T.F.; project administration, J.D.C. and T.F.; funding acquisition, E.J., F.C., and T.F. All authors have read and agreed to the published version of the manuscript.

 doi:10.20944/preprints202407.0896.v1



**Funding:** This work was funded by the Horizon 2020 research and innovation programme under the H2020 Marie Skłodowska Curie Actions grant agreement no. 813789. F.C. acknowledges his Maria Zambrano fellowship from UPV/EHU, funded by the Spanish Ministry of Universities and the European Union NextGenerationEU/PRTR, and support by grant TED2021-129299A-I00, funded by MCIU/AEI/10.13039/501100011033 and by the European Union NextGenerationEU/PRTR.

**Data availability statement:** The data supporting the reported findings as externally hosted supplementary files are openly available in the CHANGE-ITN Zenodo repository at http://doi.org/10.5281/zenodo.12656836.

**Acknowledgments:** Heartfelt thanks for discussions and contributions to Teresa Duncan (cleaning efficacy), Silvia Russo (FTIR mapping), Agnese Babini (HSI algorithms), and David Lewis (skewness). Gratitude due to Conservation Studies at UiO (lab and workshops), Guro Hjulstad at KHM (glossmeter), SciCult labs at KHM (SEM), HE-Arc CR (labs, μFTIR), LATHEMA (labs, climatic chamber), the NTNU Colourlab (HSI cameras). Further thanks to Ambra Giordano (private conservator) for her agar spray workshop that inspired this study and the encouragement to embark on it; Lena Porsmo Stoveland (conservator/researcher) for guiding mock-up production and cleaning evaluation. Final appreciation to all CHANGE-ITN colleagues for their constant support.

**Conflicts of Interest:** The authors declare no conflicts of interest. The funders had no role in the design of the study; in the collection, analyses, or interpretation of data; in the writing of the manuscript; or in the decision to publish the results.

## Appendix A: Additional Methodological Details

***Photography***. The mock-ups were photographed using a Canon 6D DSLR camera with a Canon RF 100 mm F2.8L macro IS USM lens. They were mounted upon black velvet cloth, and illuminated with Kaiser 300 W tungsten-halogen lamps under incident and raking light configurations (Table A1). Colour management was carried out using ISA RezChecker targets, which were used for white balance correction using a macro developed for ImageJ, once the RAW files had been converted to RGB images within the freeware [96,97].

This image-based metric was developed based on current trends in the literature [47]. It was found that the *L**, *a** and *b** images of the mock-ups as extracted from a CIELAB1976 colour-space gave faithful representations of the soiling upon the surfaces. This is likely since the soiling was captured as darker pixels on a lighter background (for *L**), bluer pixels on the yellowish background of the ground (for *b**), and redder pixels on the green background of the oil paint (for *a**). The RGB images were converted into their respective *L**, *a** and *b** images using the *Colour Space Converter* plug-in in ImageJ based on a D65 illuminant [98] (the developer warns against imprecisions of the plug-in – these were recognised and accepted during interpretation). The images were converted to 8-bit depth and thresholded to match the soiling pattern recorded on the mock-up surfaces. In the thres.

**Table A1.** Photography metadata recorded during documentation of the mock-up surfaces.

| ***Incident Light*** | | ***Raking Light*** | |
|---|---|---|---|
| **Image Capture** | | **Image Capture** | |
| ISO | 100 (ground); 200 (paint) | ISO | 160 (ground); 200 (paint) |
| Exposure | 1/125 s | Exposure | 1/125 s |
| Aperture | f/2.8 | Aperture | f/2.8 |
| **Setup Geometries** | | **Setup Geometries** | |
| Camera height | 73 cm | Camera height | 73 cm |
| Light quantity | 2 (left and right) | Light quantity | 1 (right) |
| Lights height from plane | 39 cm | Lights height from plane | 16 cm |
| Lights angle from plane | 45° | Lights angle from plane | 60° |
| Lights to lens distance | 45 cm | Lights to lens distance | 75 cm |

Holded images, black pixels represented soiled pixels, and white ones, cleaned pixels. For BT images, thresholding was demarcated at the image histograms' maximum, and at the best soiling representation between 60% to 80% for AT images. Cleaning efficacy was then calculated (as shown in Tables 5–6 in the main text).

 doi:10.20944/preprints202407.0896.v1



***Optical microscopy***. The mock-ups were documented in triplicate using a benchtop Leica DM2700 M Microsystem light microscope. Photomicrographs were taken using a Leica MC190 HD camera run from the Leica Application Suite v.4.13 image acquisition software. Surfaces were imaged in bright field and raking light (a Leica CLS100 lamp was used in this case) using N PLAN EPI objectives (×5/0.12 POL, and ×20/0.40 POL) at regions of interest (ROIs).

The photomicrographs were used in the assessment of two separate image-based metrics. The first was similar to the *L*a*b** metric described for photography – *L** images were used for the exposed grounds (soiling was represented as dark pixels on a bright background), and *a** images were used for the unvarnished oil paint (soiling was represented as non-green pixels on a green background).

The second metric was based on statistical moments describing image histogram distributions, following the work of Charola *et al.* [79] and Duncan *et al.* [45]. These studies used histogram skewness as a marker to monitor the removal of darker soiling on a lighter surface. In this work, Pearson's moment coefficient of skewness was used [99], as calculated by the corresponding ImageJ function. The determination was carried out for all triplicates of all mock-up categories. These values were checked for consistency in the Excel spreadsheet package by importing the image pixel values from the respective text image. The statistical descriptors (mean, mode, median, standard deviation and skewness) were in accord, with skewness moments varying between ±0.2.

The cleaning efficacy was then measured as the percentage return to the unsoiled control's skewness (as shown in Table 6 in the main text). The spreadsheet template used to calculate skewness is available online as an externally hosted supplementary file. The metric sometimes generated deviant numbers than expected, possibly since the change in skewness compared to the unsoiled reference was not always the best representative measure of cleaning efficacy for the surfaces being studied. A value of over 100% cleaning efficacy was not logical in this context, and so these values were discarded. Squaring and rooting was used to convert occasional negative values into usable positive ones, due to deviancy in the skewness calculations based on the selected controls. For these reasons, this metric should be applied with some caution.

***Glossimetry***. Gloss measurements on the mock-up surfaces were taken using an Elcometer 480 triple angle glossmeter. Based on recommendations for matte surfaces, an 85° measurement angle was used over an area of 4 mm × 55 mm. Ten readings were taken per mock-up triplicate using the *Batch* function of the glossmeter. Data was exported using the ElcoMaster 2.0 application and processed in the Excel spreadsheet package. A gloss metric was calculated as the percentage return to the unsoiled control's gloss (as explained in Table 6 in the main text).

***Hyperspectral imaging***. Spectral datacubes for each mock-up class were acquired (BT and AT) using HySpex VNIR1800 and SWIR384 pushbroom hyperspectral scanners (Norsk Elektro Optikk AS). Acquisitions were carried out following the literature [57,100,101] (Table A2). Pre-processing of the spectral cubes was carried out using the manufacturer's acquisition software, and the associated

**Table A2.** HSI acquisition conditions.

| **HSI Cameras** | ***VNIR1800*** | ***SWIR384*** | **Lights** | ***Tungsten-Halogen*** |
|---|---|---|---|---|
| Spectral range, nm | 407-998 | 951-2505 | Spectral coverage, nm | c. 320-2600 |
| Spectral bands | 186 | 288 | Quantity | 2 |
| Spectral interval[a], nm | 3.26 | 5.45 | Room lighting | Darkness |
| Pixels acquired | 1800 | 384 | Geometry[b] | 45°, h: 130 cm, d: various |
| Focal length, m | 0.30 | 0.30 | Spectral reflectance standard | Spectralon white (99%) and grey (50%) diffuse |
| Field-of-view[c], cm | 8.60 | 8.60 | | |
| Spatial resolution, μm | 50 | 220 | | |

 doi:10.20944/preprints202407.0896.v1



| Mount | Fixed, perpendicular to surface | Mount | Fixed to stage |
|---|---|---|---|
| **Acquisition Parameters** | | | |
| HSNR[d] | 0 | 0 | |
| Integration time, µs | | | |
| *for exposed ground* | 25000 | 6900 | |
| *for oil paint* | 39000 | 10800 | |

*a*: known as the full width at half maximum (FWHM) of the sensor's sensitivity distribution. *b*: *h* represents height, *d* represents distance from camera (centre SWIR camera to first light: 22.5 cm left; first light to centre VNIR camera: 15.0 cm left; centre VNIR camera to second light: 30.0 cm left). *c:* known as the ground sampling distance (GSD). *d:* HSNR is the high signal to noise ratio (i.e. the number of times each image frame is recorded and averaged).

HySpexRadV2.0 software package. Post-processing workflows were followed using the ImageJ image processing freeware package to give datacubes with reflectance values [57,102–104].

Two spectral unmixing algorithms (one semi-supervised, *PoissonNMF* [52], the other unsupervised, *LuMoS* [53]) were used to spectrally identify and map soiled and cleaned areas. The unmixing algorithms' outputs featured maps, where increasing pixel value was indicative of the degree of spectral similarity (the maps were given as 32-bit, and 16-bit images for the semi-supervised and unsupervised algorithms, respectively). The mean pixel values from 100 pixel × 100 pixel areas were used (as shown in Table 6 in the main text) to indicate percentage cleaning efficacy or percentage remainder soiling, depending on which reference area the spectral mapping was calibrated upon.

Normalised difference image (NDI) mapping was carried out as reported by Malegori *et al.* [54], Piarulli *et al.* [55], and Lugli *et al.* [56]. Using PCA [105], characteristic wavelengths in the SWIR range were selected for each mock-up's ground or oil paint surface, and for the soiling (Figure A1).

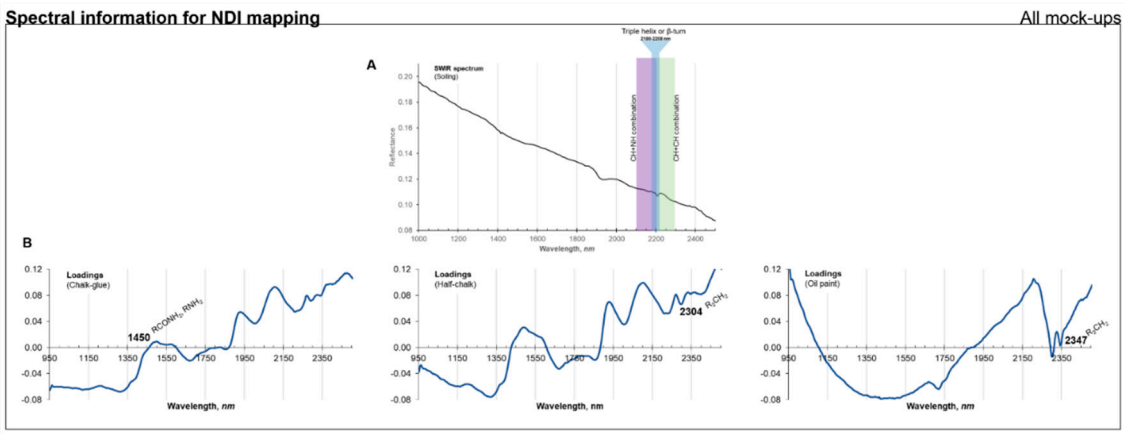


**Figure A1.** *A*. SWIR spectrum for artificial soiling and characteristic peak identified for NDI mapping (highlighted sections: CH+CN combination range in violet, CH+CH combination range in green, collagen triple helix or β-turn range in blue). *B*. PCA loading plots for the SWIR spectra of each mock-up surface, and the relevant peaks selected for NDI mapping (1 450 nm for chalk-glue ground; 2 304 nm for half-chalk ground; 2 347 nm for oil paint) [106–110].

An image difference operation was carried out with image slices corresponding to the selected wavelengths, using the *Image Calculator* function within ImageJ to execute Equation 1 in the main text. The resulting 32-bit image provided a map of the soiling upon the mock-up surface. For visualisation purposes, the images were individually adjusted for brightness and contrast to make differences more visible, and an appropriate look-up table applied. In this context, a *look-up table* is a data matrix containing information for the pixel values, and can be used to change the colour scheme of the image. The same metric as described for spectral unmixing (in Table 6 in the main text) was

 doi:10.20944/preprints202407.0896.v1



then implemented to illustrate cleaning efficacy (based on the unsoiled mock-up), or remainder of soiling (based on a soiling control). The NDI values obtained were negative, and thus Equation 1 in the main text used to calculate the percentage efficacy based on the unsoiled control was modified as shown in Equation A1 below.

$$\text{cleaning efficacy} = \left(\frac{NDI_{cleaned}}{NDI_{unsoiled}}\right) \times 100 \quad \text{(A1)}$$

This equation was derived as follows (Equations A2–A3):

$$\begin{aligned}\text{cleaning efficacy} &= \left(1 - \left(\frac{NDI_{unsoiled} - NDI_{cleaned}}{NDI_{unsoiled}}\right)\right) \times 100 \\ &= \left(1 - \left(1 - \frac{NDI_{cleaned}}{NDI_{unsoiled}}\right)\right) \times 100\end{aligned} \quad \text{(A2)}$$

$$\text{cleaning efficacy} = \frac{NDI_{cleaned}}{NDI_{unsoiled}} \times 100 \quad \text{(A3)}$$

Furthermore, to indicate the percentage soiling remaining on surfaces, the following equation (Equation A4) was used:

$$\text{cleaning efficacy} = NDI_{soiling}/NDI_{cleaned} \quad \text{(A4)}$$

Images of the NDI maps of the cleaned mock-ups were opened in ImageJ, converted to 8-bit depth (required by the plug-in), and analysed with the *GLCM Texture* plug-in, using a pixel step of 1 in the 0º direction. The value given for the inverse difference moment was taken as a homogeneity score, where a value of 1 represented an entirely homogenous image (all pixels have the same intensity), and therefore fully homogeneous cleaning (the equations used to calculate image homogeneity can be found in Albregtsen [90]).

The initial presumed overlap between mock-up and soiling identifiers was recognised, especially since considerable band overlap is common in the SWIR. For example, although collagen and gelatine, two highly similar macromolecules, each contain identical functional groups, their chemically diverse environs will have resulted in different band contributions – this has been confirmed by PCA in this case [57], and conceptually [111,112]. Furthermore, Duconseille *et al*. [108] confirm that aged gelatines (such as in the chalk-glue ground) have higher NH overtone vibrations than non-aged gelatines (such as in the soiling's gelatine), which feature more prominent CH+NH combination modes. For the chalk-glue ground, an attempt to use the SWIR bands for calcite (which were marked by PCA as significant) was unsuccessful, most likely due to interference from bands from other materials: two clusters resulted on the score plots representing soiled and unsoiled surfaces distinctly. The loading plots indicated that the calcite bands should be contributing to the observed variance. These bands were at 1997 $cm^{-1}$, and 2340 $cm^{-1}$. They conflicted with proximal bands at 2009 $cm^{-1}$ and 2342 $cm^{-1}$ (associated with the gelatine, and linseed oil in the mock-ups respectively), and did not give sufficiently coherent NDI maps.

***Colorimetry from HSI.*** A relatively quick, simplified method for calculating colour change was implemented based on selecting three bands (corresponding to R, G, B channels) from the HSI datacube. The latter is a quick way to visualise a colour image from spectral data. As such it can be useful, but it is acknowledged that it is not a fully colorimetric method. Further colorimetric analyses in CIELAB could be carried out through the convolution of image data with XYZ colour-matching functions [113] (a comparison of these two methods was beyond the scope of this paper).

In ImageJ, *L*a*b** values for the mock-up surfaces were generated as follows: a sub-stack of three slices from the red, green and blue spectral regions of the datacube was produced at 16-bit depth. The three slices used were taken from the bands at 647.9, 552.2, and 466.0 nm for R, G, B channels respectively. The stack was then converted into an RGB image, and subsequently converted into separate *L**, *a**, *b** images using the *Colour Space Converter* plug-in, specifying a D65 illuminant. The three images were then reconverted into a stack, and respective *L*a*b** values extracted from its *z*-axis profile.

 doi:10.20944/preprints202407.0896.v1



Ten ROIs measuring 100 pixels × 100 pixels were used to extract the $L^*a^*b^*$ values for each mock-up, and processed in the Excel spreadsheet package to calculate mean and coefficient of variation values. Deviating measurements were discarded using the ISO-recommended Grubbs' test at $P = 0.05$ [114]. The formula used to measure the colour difference, $\Delta E$, was the CIEDE2000 equation [115,116], using the calculator developed by Boronkay [117]. Error propagation was calculated according to Miller & Miller [114] and Williams [118]. The spreadsheet template used to calculate error propagation with $L^*a^*b^*$ values is available online as an externally hosted supplementary file. Propagation calculations were confirmed using the Error Propagation Calculator application [119]. Using these values, a colorimetry metric was calculated as the percentage return to the unsoiled control's colour (as shown in Table 6 in the main text).

No cleaned mock-up matched the colour nor tone of the unsoiled control: this was recognised as a highly idealistic comparison given that the surface would have continued changing during ageing. The colorimetry metric thus helped appreciate this change numerically, but was based on return to the unsoiled control, and this should be borne in mind whilst evaluating results.

***μFTIR mapping.*** Fourier-transform infrared (FTIR) 2D chemical maps of ROIs on the mock-ups were collected using a ThermoScientific Nicolet iNTM10 MX FTIR microscope, equipped with a motorised *xyz*-stage. Each ROI consisted of 350 16-scan spectra collected over 5 s in attenuated total reflectance (ATR) mode (Germanium-crystal, liquid nitrogen-cooled detector, 15 arbitrary pressure units) over the range 4000–650 $cm^{-1}$, using an aperture of 150 μm × 150 μm, a step size of 100 μm, and 4 $cm^{-1}$ resolution, over a total surface area of 3500 μm × 1000 μm.

ATR was used as the mode of acquisition, since spectra acquired in diffuse reflectance suffered badly from different interactions of the IR radiation with the surface, probably as a result of the non-uniform and non-homogeneous topography of the soiling [120]. As the mock-ups were expendable, the increased contact with the ATR crystal was not an issue, however, the presence of soot (carbon black) particles in the soiling mixture meant that at certain points in the maps, background noise was registered, influencing the quality of the maps. This is possibly due to the higher refractive index of carbon black (compared to other organic materials), which, despite the higher refractive index of the germanium crystal, might have still led to light being transmitted into the sample, creating band distortions via anomalous dispersion that present as asymmetric spectral artefacts [121]. Raman point analysis carried out separately to this study confirmed these points did contain carbon.

Visualisation of single spectra was carried out in Spectragryph 1.2.15 [122]. Pre-processing of the maps was limited to atmospheric corrections for carbon dioxide and water as carried out in Omnic 9.2.86. Post-processing began with background subtraction of the mock-up surface to intensify the soiling signal. Soiling maps were then generated using the *Correlation map* profile feature in Omnic Atlμs 9.2.91, and were based on spectral similarity to the artificial soiling's spectrum. The intensity of pixels in the soiling maps corresponded to increasing spectral matches to the molecular fingerprint of the soiling.

The latter maps were exported as greyscale .tiff files into ImageJ, assigned the desired look-up table and adjusted for brightness and contrast to improve visualisation. The images were then automatically thresholded and converted to 8-bit binary images, so that black pixels represented cleaned areas (no soiling spectrum detected), whereas white pixels represented soiled areas (any degree of soiling spectrum detected). The percentage cleaning efficacy as measured by FTIR was then calculated (following Table 6 in the main text).

***SEM imaging and SEM-EDX mapping***. The mock-up surfaces were investigated by scanning electron microscopy (SEM) using a FEI Quanta 450 electron microscope equipped with an X-Max Oxford 50 $mm^2$ SSD detector, running on Aztec 3.1 SP1 software. Each mock-up (c. 5 cm × 5 cm) was mounted on the stage of the vacuum chamber with carbon tape and no surface preparation. The same ROIs as for microscopy and FTIR were used. A slightly different area was imaged however for SEM, as the ATR diamond disrupted the surface (Figure A2), preventing monitoring. The methodology employed implied that the acquisition process was quasi-non-contact (except for the attaching of conductive tape to the back of the mock-up). It should be borne in mind that alteration of the surface

 doi:10.20944/preprints202407.0896.v1



is technically possible by charge accumulation, which can shift particles around, or by burning through the surface via high electron flux (e.g. when using high acceleration voltages [123–125].

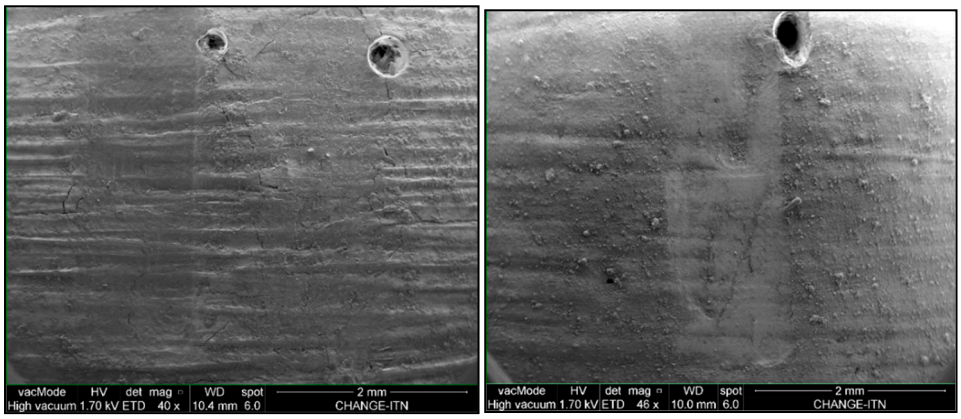


**Figure A2.** Disruption of the mock-up surfaces and soiling by the ATR diamond (*left*: ground; *right*: oil paint). AT measurements were taken from the area immediately below, as shown on the right.

The following conditions were used for imaging based on procedures in the literature and recommendations for unvarnished painted surfaces [123,124,126]: secondary electron (SE) images were acquired at ×100, ×500 and ×1000 in high vacuum mode with an Everhart-Thornley (ETD) detector at low acceleration voltage (1.7 kV), a working distance of c. 10 mm, with a beam spot size of 6.0 mm². The magnification and contrast for each mock-up was slightly adjusted in order to obtain the sharpest image. SEM-EDX was carried on back-scattered electron (BSE) images acquired at ×500 in low-vacuum mode with a circular backscatter (CBS) detector at high acceleration voltage (20.0 kV), with the same working distance, and electron beam spot size. Element maps were processed using the TruMap feature within the Aztec® software (only the mock-ups cleaned by the citrate/$NH_4OH$ solution were mapped due to project restrictions).

After being identified as indicative markers of the artificial soiling used, Al and Si element maps were selected for use in the SEM-EDX-based metric for cleaning efficacy (Figure A3). The maps were imported into FIJI (ImageJ) as .tiff files and converted into 8-bit binary images that were automatically thresholded (applying the *Fill Holes* option to create distinct particulate units). Al- and Si-containing areas were represented as white pixels in this manner. The *Analyse Particles* function was then used to count individual, defined areas, and used to calculate cleaning efficacy (as listed in Table 6 in the main text).

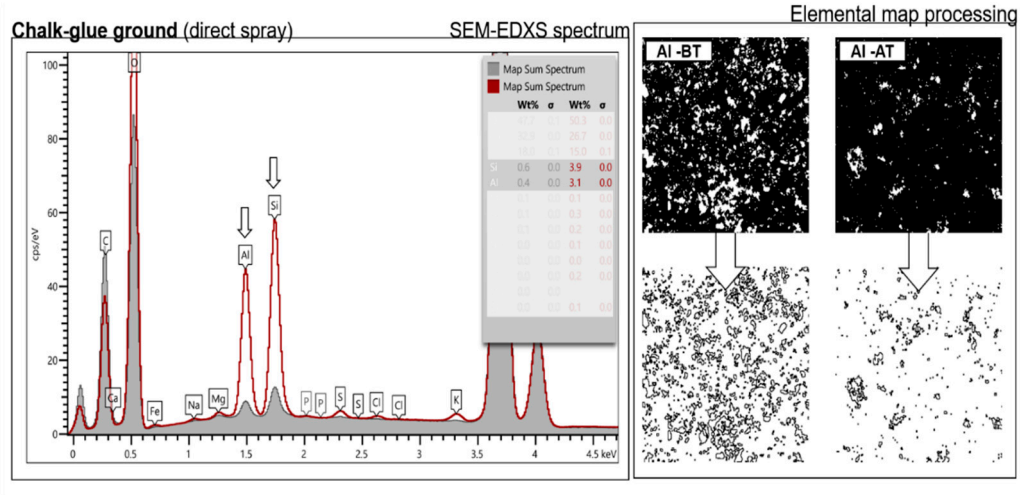


**Figure A3.** An example comparison of SEM-EDX spectra showing the marked change in counts for Al and Si after cleaning (*left*). An example of the thresholded maps and their relevant defined area counting output (*right)*.

 doi:10.20944/preprints202407.0896.v1



***Treatment evaluation scores***. An image-based and spectral-based efficacy score were generated as an average of the cleaning efficacy values for each class of metric. For the image-based efficacy, the *L*a*b** metric at the microscale and the skewness metric were considered. The total cleaning efficacy used for the scoring criteria was then calculated as a further average of these two values. For the spectral-based efficacy, the values from the semi-supervised unmixing in the VNIR, the NDI mapping in the SWIR, and the FTIR mapping in the MIR were selected, following the recommendations given in the main text, and permitting the score to cover a large swathe of the electromagnetic spectrum. Cleaning homogeneity was taken from the result of the GLCM analysis. The colorimetry and gloss metric values were fed directly into the colour and gloss integrity score fields, as they formed independent criteria for evaluation. Finally, the scores for cleaning selectivity (lack of pigment loss) and residue absence were evaluated by eye during real-time observations, and were broken down into five incremental divisions (0.2 being worst, and 1.0 being best). The absence of residues was not included as a scoring criterion, as all cleaning tests had scored the best possible score, i.e. no residues were noticed when the agar technique was applied correct.

## Appendix B: Discussion of Unsupervised Unmixing for Soiling Removal Mapping

For comparison purposes, the unsupervised unmixing algorithm was tested for mapping soiling removal. Compared to the semi-supervised algorithm (which searched for what the user specified [52]), it did not require the input of guiding regions of interest (ROIs) associated with clean or soiled areas. Although an expected number of different spectral regions was inputted as guidance, it is the algorithm that grouped all spectra into different classes, and mapped similar areas accordingly [53].

The unsupervised unmixing algorithm applied to the exposed grounds resulted in somewhat inconsistent mapping for both the VNIR and SWIR ranges, particularly when attempting to map soiled areas (the algorithm did not seem to identify these surfaces as spectrally distinguishable). Mapping of cleaned areas was successful, although false positives were noted for soiling references. In this case, the general trends for soiling removal by the chelating agent observed in the VNIR range with the semi-supervised algorithm also applied here: the chalk-glue ground was almost fully cleaned, the half-chalk ground was notably less cleaned, and the oil paint was cleaned most.

Cleaning efficacy plots based on the unsupervised algorithm are given in Figure B1. Notably, this algorithm reported the surfaces as more soiled in the SWIR range. According to calculations based on SWIR data, the spray and pre-formed gel had similar performances, with the citrate/$NH_4OH$ solution performing notably better for the chalk-glue ground, and only marginally better for the half-chalk ground. The cleaning efficacy by spray was more marked for the oil paint than by pre-formed gel, with chelation giving markedly better results. All these results matched visual observations better than the VNIR counterparts.

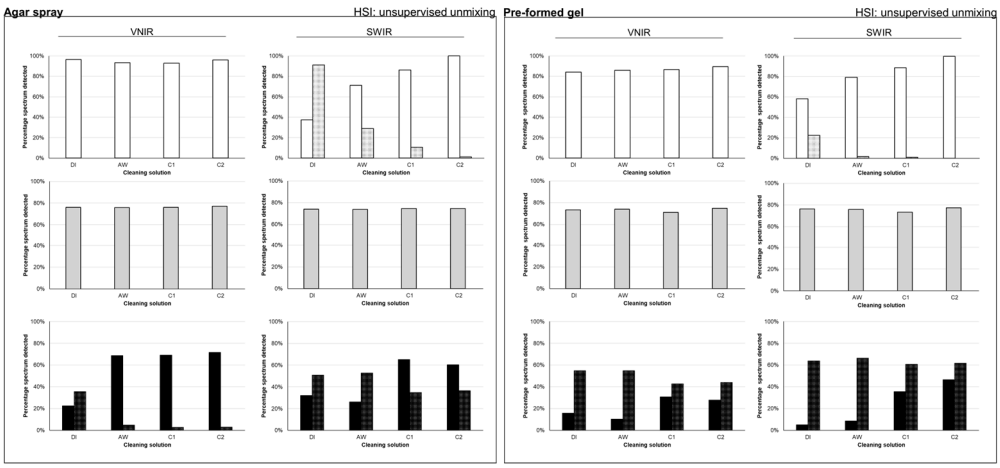


**Figure A4.** VNIR and SWIR metric plots as determined by the unsupervised unmixing algorithm, based on clean (plain fill) and soiled (textured fill) reference spectra for spray-cleaned surfaces (*left*) and the pre-formed gel cleaning (*bottom*). Error bars not plotted since RSD ranged between 1.00 and

 doi:10.20944/preprints202407.0896.v1



13.86 in many cases; soiling was not detected on the half-chalk ground, and sprayed chalk-glue ground (keys: white – chalk-glue; grey – half-chalk; black – chromium oxide • (DI) deionised water; (AW) adjusted water; (C1) citric acid in NaOH solution; (C2) citric acid in $NH_4OH$ solution).

However, the limited reliability of the unsupervised method did not make it ideal for assessing soiling removal. The relative standard deviation (RSD) for the cleaning efficacy values in half of the plots was large enough to cast doubt on the results (RSD for chalk-glue ground: 0.07–13.86%; RSD for half-chalk ground: 0.06–0.08%; RSD for oil paint: 0.55–5.83%); whereas soiling was at times not even detected. Should it be used, the VNIR range is recommended, keeping in mind that this algorithm was designed for pigment identification [75], rather than mapping areas of cleaned and soiled surfaces.

## References


1. Ormsby, B.; Bartoletti, A.; van den Berg, K. J.; Stavroudis, C. Cleaning and Conservation: Recent Successes and Challenges. *Heritage Science*, **2024**, *12* (1), 10. https://doi.org/10.1186/s40494-023-01113-0.
2. *Dirt and Dirt Removal | Paintings Conservation*; Van den Berg, K. J., Gorter, L., Eds.; Paintings Conservation; Cultural Heritage Agency Netherlands: Amersfoort, 2022.
3. Passaretti, A.; Cuvillier, L.; Sciutto, G.; Guilminot, E.; Joseph, E. Biologically Derived Gels for the Cleaning of Historical and Artistic Metal Heritage. *Applied Sciences*, **2021**, *11* (8), 3405. https://doi.org/10.3390/app11083405.
4. Angelova, L. V.; Ormsby, B.; Townsend, J.; Wolbers, R. *Gels in the Conservation of Art*; Archetype Publications, 2017.
5. Mastrangelo, R.; Montis, C.; Bonelli, N.; Tempesti, P.; Baglioni, P. Surface Cleaning of Artworks: Structure and Dynamics of Nanostructured Fluids Confined in Polymeric Hydrogel Networks. *Phys. Chem. Chem. Phys.*, **2017**, *19* (35), 23762–23772. https://doi.org/10.1039/C7CP02662E.
6. *Issue S1: Proceedings of the LACONA 10 Conference, Sharjah 2014, August 2015*; Elnaggar, A., Nevin, A., Castillejo, M., Strlič, M., Eds.; Routledge: Studies in Conservation, 2015.
7. Alabone, G.; Carvajal, M. S. The Removal of Bronze Paint Repairs from Overgilded Picture Frames Using an Erbium:YAG Laser. *Journal of the Institute of Conservation*, **2020**, *43* (1), 107–121. https://doi.org/10.1080/19455224.2019.1706595.
8. Duncan, T. T.; Chan, E. P.; Beers, K. L. Maximizing Contact of Supersoft Bottlebrush Networks with Rough Surfaces to Promote Particulate Removal. *ACS Appl. Mater. Interfaces*, **2019**, *11* (48), 45310–45318. https://doi.org/10.1021/acsami.9b17602.
9. Freese, S.; Diraoui, S.; Mateescu, A.; Frank, P.; Theodorakopoulos, C.; Jonas, U. Polyolefin-Supported Hydrogels for Selective Cleaning Treatments of Paintings. *Gels*, **2019**, *6* (1), 1. https://doi.org/10.3390/gels6010001.
10. Bartoletti, A.; Barker, R.; Chelazzi, D.; Bonelli, N.; Baglioni, P.; Lee, J.; Angelova, L. V.; Ormsby, B. Reviving WHAAM! A Comparative Evaluation of Cleaning Systems for the Conservation Treatment of Roy Lichtenstein's Iconic Painting. *Herit Sci*, **2020**, *8* (1), 9. https://doi.org/10.1186/s40494-020-0350-2.
11. Mastrangelo, R.; Chelazzi, D.; Poggi, G.; Fratini, E.; Pensabene Buemi, L.; Petruzzellis, M. L.; Baglioni, P. Twin-Chain Polymer Hydrogels Based on Poly(Vinyl Alcohol) as New Advanced Tool for the Cleaning of Modern and Contemporary Art. *Proc Natl Acad Sci U S A*, **2020**, *117* (13), 7011–7020. https://doi.org/10.1073/pnas.1911811117.
12. Sansonetti, A.; Bertasa, M.; Canevali, C.; Rabbolini, A.; Anzani, M.; Scalarone, D. A Review in Using Agar Gels for Cleaning Art Surfaces. *Journal of Cultural Heritage*, **2020**, *44*, 285–296.
13. Al-Emam, E.; Motawea, A. G.; Caen, J.; Janssens, K. Soot Removal from Ancient Egyptian Complex Painted Surfaces Using a Double Network Gel: Empirical Tests on the Ceiling of the Sanctuary of Osiris in the Temple of Seti I—Abydos. *Heritage Science*, **2021**, *9* (1), 1–10.
14. Bertasa, M.; Canevali, C.; Sansonetti, A.; Lazzari, M.; Malandrino, M.; Simonutti, R.; Scalarone, D. An In-Depth Study on the Agar Gel Effectiveness for Built Heritage Cleaning. *Journal of Cultural Heritage*, **2021**, *47*, 12–20.
15. Giordano, A.; Cremonesi, P. New Methods of Applying Rigid Agar Gels: From Tiny to Large-Scale Surface Areas. *Studies in Conservation*, **2021**, *66* (8), 437–448. https://doi.org/10.1080/00393630.2020.1848272.
16. Jia, Y.; Sciutto, G.; Botteon, A.; Conti, C.; Focarete, M. L.; Gualandi, C.; Samorì, C.; Prati, S.; Mazzeo, R. Deep Eutectic Solvent and Agar: A New Green Gel to Remove Proteinaceous-Based Varnishes from Paintings. *Journal of Cultural Heritage*, **2021**, *51*, 138–144. https://doi.org/10.1016/j.culher.2021.08.001.
17. Stoveland, L. P.; Frøysaker, T.; Stols-Witlox, M.; Grøntoft, T.; Steindal, C. C.; Madden, O.; Ormsby, B. Evaluation of Novel Cleaning Systems on Mock-Ups of Unvarnished Oil Paint and Chalk-Glue Ground

within the Munch Aula Paintings Project. *Herit Sci*, **2021**, *9* (1), 144. https://doi.org/10.1186/s40494-021-00599-w.

18. Giordano, A.; Caruso, M. R.; Lazzara, G. New Tool for Sustainable Treatments: Agar Spray—Research and Practice. *Heritage Science*, **2022**, *10* (1), 123. https://doi.org/10.1186/s40494-022-00756-9.
19. Delattre, C.; Bearman, G.; Choi, Y. L.; McPherson, L.; Stiglitz, M. The Use of Enzymatic Gels in the Conservation Treatment of Mendelssohn's "Green Books." In *ICOM-CC 20th Triennial Conference Preprints Valencia 18-22 September 2023*; ICOM: Paris, 2023; pp 1–8.
20. Husby, L. M.; Andersen, C. K.; Pedersen, N. B.; Ormsby, B. Selecting, Modifying, and Evaluating of Water-Based Methods for the Removal of Dammar Varnish from Oil Paint. *Meddelelser om Konservering*, **2023**, *2023*, 51–65.
21. Husby, L. M.; Andersen, C. K.; Pedersen, N. B.; Ormsby, B. Evaluating Three Water-Based Systems and One Organic Solvent for the Removal of Dammar Varnish from Artificially Aged Oil Paint Samples. *Heritage Science*, **2023**, *11* (1), 244. https://doi.org/10.1186/s40494-023-01077-1.
22. Ortiz Miranda, A. S.; Lehmann Banke, P.; Ludvigsen, L. Non-Invasive Imaging Systems as Tools for Evaluating Treatments: The Case "Bathers" by Henri Matisse. In *ICOM-CC 20th Triennial Conference Preprints Valencia 18-22 September 2023*; Bridgland, J., Ed.; ICOM: Paris, 2023; pp 1–11.
23. Tobin, G.; Sawicki, M. Developing Conservation Practices for Cleaning Gilded Surfaces: Application for xPVOH-Borax Organogels to Clean Two Gilded Frames. In *ICOM-CC 20th Triennial Conference Preprints Valencia 18-22 September 2023*; Bridgland, J., Ed.; ICOM: Paris, 2023; pp 1–16.
24. Cuvillier, L.; Passaretti, A.; Guilminot, E.; Joseph, E. Agar and Chitosan Hydrogels' Design for Metal-Uptaking Treatments. *Gels*, **2024**, *10* (1), 55. https://doi.org/10.3390/gels10010055.
25. Macchia, A.; Biribicchi, C.; Carnazza, P.; Montorsi, S.; Sangiorgi, N.; Demasi, G.; Prestileo, F.; Cerafogli, E.; Colasanti, I. A.; Aureli, H.; et al. Multi-Analytical Investigation of the Oil Painting "Il Venditore Di Cerini" by Antonio Mancini and Definition of the Best Green Cleaning Treatment. *Sustainability*, **2022**, *14* (7), 3972. https://doi.org/10.3390/su14073972.
26. Frøysaker, T. Unintended Contamination? A Selection of Munch's Paintings with Non-Original Zinc White. In *Public paintings by Edvard Munch and his contemporaries. Change and conservation challanges*; Frøysaker, T., Streeton, N. L. W., Kutzke, H., Hanssen-Bauer, F., Topalova-Casadiego, B., Eds.; Archetype Publications: London, 2015; pp 132–140.
27. Daudin-Schotte, M.; Bisschoff, M.; Joosten, I.; Keulen, H. van; Berg, K. J. van den. Dry Cleaning Approaches for Unvarnished Paint Surfaces. In *New Insights into the Cleaning of Paintings: Proceedings from the Cleaning 2010 International Conference Universidad Politécnica de Valencia and Museum Conservation Institute*; Mecklenburg, M., Charola, A. E., Koestler, R. J., Eds.; Smithsonian Institution Scholary Press: Washington D.C., 2013; pp 209–219.
28. Gillman, M.; Lee, J.; Ormsby, B.; Burnstock, A. Water-Sensitivity in Modern Oil Paintings: Trends in Phenomena and Treatment Options. In *Conservation of Modern Oil Paintings*; van den Berg, K. J., Bonaduce, I., Burnstock, A., Ormsby, B., Scharff, M., Carlyle, L., Heydenreich, G., Keune, K., Eds.; Springer International Publishing: Cham, 2019; pp 477–494. https://doi.org/10.1007/978-3-030-19254-9_37.
29. Ormsby, B.; Lee, J.; Bonaduce, I.; Lluveras-Tenorio, A. Evaluating Cleaning Systems for Use on Water Sensitive Modern Oil Paints: A Comparative Study. In *Conservation of Modern Oil Paintings*; van den Berg, K. J., Bonaduce, I., Burnstock, A., Ormsby, B., Scharff, M., Carlyle, L., Heydenreich, G., Keune, K., Eds.; Springer International Publishing: Cham, 2019; pp 11–35. https://doi.org/10.1007/978-3-030-19254-9_2.
30. Bartoletti, A.; Maor, T.; Chelazzi, D.; Bonelli, N.; Baglioni, P.; Angelova, L. V.; Ormsby, B. A. Facilitating the Conservation Treatment of Eva Hesse's Addendum through Practice-Based Research, Including a Comparative Evaluation of Novel Cleaning Systems. *Heritage Science*, **2020**, *8* (1), 35. https://doi.org/10.1186/s40494-020-00378-z.
31. Chung, J. Y.; Ormsby, B.; Lee, J.; Burnstock, A. An Investigation of Options for Surface Cleaning Unvarnished Water- Sensitive Oil Paints Based on Recent Developments for Acrylic Paints. **2017**, 12.
32. Sully, D. Conservation Theory and Practice: Materials, Values, and People in Heritage Conservation. In *The International Handbooks of Museum Studies*; John Wiley & Sons, Ltd, 2015; pp 293–314. https://doi.org/10.1002/9781118829059.wbihms988.
33. Cutajar, J. D.; Duckor, A.; Sully, D.; Fredheim, L. H. A Significant Statement: New Outlooks on Treatment Documentation. *Journal of the Institute of Conservation*, **2016**, *39* (2), 81–97. https://doi.org/10.1080/19455224.2016.1212717.
34. Fredheim, L. H.; Khalaf, M. The Significance of Values: Heritage Value Typologies Re-Examined. *International Journal of Heritage Studies*, **2016**, *22* (6), 466–481.
35. Avrami, E.; Mason, R. Mapping the Issue of Values. Values in heritage management. Emerging approaches and research directions, **2019**, 9–33.
36. Lithgow, K.; Golfomitsou, S.; Dillon, C. Coming Clean about Cleaning. Professional and Public Perspectives: Are Conservators Truthful and Visitors Useful in Decision-Making? *Studies in Conservation*, **2018**, *63* (sup1), 392–396. https://doi.org/10.1080/00393630.2018.1479929.

37. Coming Clean http://www.comingcleanucl.com (accessed Oct 29, 2022).
38. Carlyle, L.; Witlox, M. Historically Accurate Reconstructions of Artists' Oil Painting Materials. *Tate Papers*, **2005**, *7* (1), 1–9.
39. Carlyle, L. Historically Accurate Reconstructions of Oil Painters Materials: An Overview of the HART Project 2002-2005. In Reporting Highlights of the De Mayerne Programme: Research programme on molecular studies in conservation and technical studies in history; Ferreira, E. S. B., Jaap, J. B., Eds.; Netherlands Organisation for Scientific Research: The Hague, 2006; pp 63–76.
40. Lawson, L.; Cane, S. Do Conservators Dream of Electric Sheep? Replicas and Replication. *Studies in Conservation*, **2016**, *61* (sup2), 109–113. https://doi.org/10.1080/00393630.2016.1181348.
41. Pugliese, M.; Ferriani, B.; Ratti, I. Materiality and Immateriality in Lucio Fontana's Environments: From Documentary Research to the Reproduction of Lost Artworks. *Studies in Conservation*, **2016**, *61* (sup2), 188–192. https://doi.org/10.1080/00393630.2016.1181925.
42. Stoveland, L. P.; Ormsby, B.; Stols-Witlox, M.; Frøysaker, T.; Caruso, F. Designing Paint Mock-Ups for a Study of Novel Surface Cleaning Techniques for Munch's Unvarnished Aula Paintings. In *Conservation of Modern Oil Paintings*; van den Berg, K. J., Bonaduce, I., Burnstock, A., Ormsby, B., Scharff, M., Carlyle, L., Heydenreich, G., Keune, K., Eds.; Springer International Publishing: Cham, 2019; pp 553–563. https://doi.org/10.1007/978-3-030-19254-9_41.
43. Stoveland, L. P.; Stols-Witlox, M.; Ormsby, B.; Streeton, N. L. W. Mock-Ups and Materiality in Conservation Research. In *Transcending boundaries: integrated approaches to conservation. ICOM-CC 19th triennial conference Beijing preprints*; Bridgland, J., Ed.; ICOM-CC: Beijing, 2021; pp 1–14.
44. Frøysaker, T.; Miliani, C.; Grøntoft, T.; Kleiva, I. Monitoring of Surface Blackening and Zinc Reaction Products on Prepared Samples Located Adjacent to Munch's The Source in the Aula at the University of Oslo. In *Public paintings by Edvard Munch and his contemporaries. Change and conservation challanges*; Frøysaker, T., Streeton, N. L. W., Kutzke, H., Hanssen-Bauer, F., Topalova-Casadiego, B., Eds.; Archetype Publications: London, 2015; pp 126–131.
45. Duncan, T. T.; Vicenzi, E. P.; Lam, T.; Brogdon-Grantham, S. A. A Comparison of Dry-Cleaning Materials for the Removal of Soot from Rough Papers: *Journal of the American Institute for Conservation*, **2023**, 39.
46. Striova, J.; Dal Fovo, A.; Fontana, R. Reflectance Imaging Spectroscopy in Heritage Science. *Riv. Nuovo Cim.*, **2020**, *43* (10), 515–566. https://doi.org/10.1007/s40766-020-00011-6.
47. Duncan, T. T.; Chan, E. P.; Beers, K. L. Quantifying the 'Press and Peel' Removal of Particulates Using Elastomers and Gels. *Journal of Cultural Heritage*, **2021**, *48*, 236–243. https://doi.org/10.1016/j.culher.2020.11.004.
48. Schindelin, J.; Arganda-Carreras, I.; Frise, E.; Kaynig, V.; Longair, M.; Pietzsch, T.; Preibisch, S.; Rueden, C.; Saalfeld, S.; Schmid, B.; et al. Fiji: An Open-Source Platform for Biological-Image Analysis. *Nat Methods*, **2012**, *9* (7), 676–682. https://doi.org/10.1038/nmeth.2019.
49. Drumetz, L.; Chanussot, J.; Jutten, C. Chapter 2.7 - Variability of the Endmembers in Spectral Unmixing. In *Data Handling in Science and Technology*; Amigo, J. M., Ed.; Elsevier, 2020; Vol. 32, pp 167–203. https://doi.org/10.1016/B978-0-444-63977-6.00009-2.
50. Nascimento, J.; Martín, G. Chapter 2.6 - Nonlinear Spectral Unmixing. In *Data Handling in Science and Technology*; Amigo, J. M., Ed.; Elsevier, 2020; Vol. 32, pp 151–166. https://doi.org/10.1016/B978-0-444-63977-6.00008-0.
51. Quintano, C.; Fernández-Manso, A.; Shimabukuro, Y. E.; Pereira, G. Spectral Unmixing. *International Journal of Remote Sensing*, **2012**, *33* (17), 5307–5340. https://doi.org/10.1080/01431161.2012.661095.
52. Neher, R. A.; Mitkovski, M.; Kirchhoff, F.; Neher, E.; Theis, F. J.; Zeug, A. Blind Source Separation Techniques for the Decomposition of Multiply Labeled Fluorescence Images. *Biophysical Journal*, **2009**, *96* (9), 3791–3800. https://doi.org/10.1016/j.bpj.2008.10.068.
53. McRae, T. D.; Oleksyn, D.; Miller, J.; Gao, Y.-R. Robust Blind Spectral Unmixing for Fluorescence Microscopy Using Unsupervised Learning. *PLOS ONE*, **2019**, *14* (12), e0225410. https://doi.org/10.1371/journal.pone.0225410.
54. Malegori, C.; Alladio, E.; Oliveri, P.; Manis, C.; Vincenti, M.; Garofano, P.; Barni, F.; Berti, A. Identification of Invisible Biological Traces in Forensic Evidence by Hyperspectral NIR Imaging Combined with Chemometrics. *Talanta*, **2020**, *215*, 120911. https://doi.org/10.1016/j.talanta.2020.120911.
55. Piarulli, S.; Sciutto, G.; Oliveri, P.; Malegori, C.; Prati, S.; Mazzeo, R.; Airoldi, L. Rapid and Direct Detection of Small Microplastics in Aquatic Samples by a New near Infrared Hyperspectral Imaging (NIR-HSI) Method. *Chemosphere*, **2020**, *260*, 127655. https://doi.org/10.1016/j.chemosphere.2020.127655.
56. Lugli, F.; Sciutto, G.; Oliveri, P.; Malegori, C.; Prati, S.; Gatti, L.; Silvestrini, S.; Romandini, M.; Catelli, E.; Casale, M.; et al. Near-Infrared Hyperspectral Imaging (NIR-HSI) and Normalized Difference Image (NDI) Data Processing: An Advanced Method to Map Collagen in Archaeological Bones. *Talanta*, **2021**, *226*, 122126. https://doi.org/10.1016/j.talanta.2021.122126.

57. Cutajar, J. D.; Babini, A.; Deborah, H.; Hardeberg, J. Y.; Joseph, E.; Frøysaker, T. Hyperspectral Imaging Analyses of Cleaning Tests on Edvard Munch's Monumental Aula Paintings. *Studies in Conservation*, **2022**, *67* (sup1), 59–68. https://doi.org/10.1080/00393630.2022.2054617.
58. CHANGE https://change-itn.eu/ (accessed Jul 1, 2024).
59. The Munch Aula Paintings project (MAP) - Department of Archaeology, Conservation and History https://www.hf.uio.no/iakh/english/research/projects/aula-project/index.html (accessed Jul 1, 2024).
60. Lee, J.; Ormsby, B.; Burnstock, A.; van den Berg, K. J. Modern Oil Paintings in Tate's Collection: A Review of Analytical Findings and Reflections on Water-Sensitivity. In *Conservation of Modern Oil Paintings*; van den Berg, K. J., Bonaduce, I., Burnstock, A., Ormsby, B., Scharff, M., Carlyle, L., Heydenreich, G., Keune, K., Eds.; Springer International Publishing: Cham, 2019; pp 495–522. https://doi.org/10.1007/978-3-030-19254-9_38.
61. Frøysaker, T. The Paintings of Edvard Munch in the Assembly Hall of Oslo University. Their Treatment History and the Aula-Project. *Restauro. Forum für Restauratoren, Konservatoren und Denkmalpfleger*, **2007**, *113* (4), 246–257.
62. Frøysaker, T.; Liu, M. Four (of Eleven) Unvarnished Oil Paintings on Canvas by Edvard Munch in the Aula of Oslo University. Preliminary Notes on Their Materials, Techniques and Original Appearances. *Restauro. Forum für Restauratoren, Konservatoren und Denkmalpfleger*, **2009**, *115* (1), 44–62.
63. Frøysaker, T.; Miliani, C.; Liu, M. Non-Invasive Evaluation of Cleaning Tests Performed on "Chemistry" (1909-1916). A Large Unvarnished Oil Painting on Canvas by Edvard Munch. *Restauro. Forum für Restauratoren, Konservatoren und Denkmalpfleger*, **2011**, *117* (4), 53–63.
64. Frøysaker, T.; Liu, M.; Miliani, C. Extended Abstract—Noninvasive Assessments of Cleaning Tests on an Unvarnished Oil Painting on Canvas by Edvard Munch. In *New Insights into the Cleaning of Paintings: Proceedings from the Cleaning 2010 International Conference, Universidad Politécnica de Valencia and Museum Conservation Institute*; Mecklenburg, M., Charola, A. E., Koestler, R. J., Eds.; Smithsonian Institution Scholary Press: Washington D.C., 2013; pp 119–123.
65. Mengshoel, K.; Liu, M.; Kempton, H. M.; Frøysaker, T. Moving Monumental Munch: From Listed Building to Temporary Studio - and Back Again. In *Moving Collections. Processes and Consequences*; Bronken, I. A. T., Braovac, S., Olstad, T. M., Ørnhøi, A. A., Eds.; Archetype Publications: London, 2012; pp 65–72.
66. Scharffenberg, K. S. Investigations of a Tideline and Its Influences on the Painting Materials in The Source. In *Public paintings my Edvard Munch and his contemporaries. Change and conservation challanges*; Frøysaker, T., Streeton, N. L. W., Kutzke, H., Hanssen-Bauer, F., Topalova-Casadiego, B., Eds.; Archetype Publications: London, 2015; pp 117–125.
67. Frøysaker, T.; Schönemann, A.; Gernert, U.; Stoveland, L. P. Past and Current Examinations of Ground Layers in Edvard Munch's Canvas Paintings. *Journal of Art Technology and Conservation*, **2019**, *34* (2), 285–300.
68. Ormsby, B.; Soldano, A.; Keefe, M.; Phenix, A.; Learner, T. An Empirical Evaluation of a Range of Cleaning Agents for Removing Dirt from Artist's Acrylic Emulsion Paints. In *The AIC Painting Specialty Group Postprints. Volume 23, 2010.*; Buckley, B., Ed.; AIC: Washington D.C., 2013; pp 77–87.
69. Stoveland, L. P.; Ormsby, B.; Stols-Witlox, M.; Frøysaker, T.; Caruso, F. Designing Paint Mock-Ups for a Study of Novel Surface Cleaning Techniques for Munch's Unvarnished Aula Paintings. In *Conservation of Modern Oil Paintings*; van den Berg, K. J., Bonaduce, I., Burnstock, A., Ormsby, B., Scharff, M., Carlyle, L., Heydenreich, G., Keune, K., Eds.; Springer International Publishing: Cham, 2019; pp 553–563. https://doi.org/10.1007/978-3-030-19254-9_41.
70. Mills, L.; Burnstock, A.; Keulen, H.; Duarte, F.; Megens, L.; Van den Berg, K. J. Water Sensitivity of Modern Artists' Oil Paints. In *ICOM Committee for Conservation, 15th Triennial Meeting*; ICOM-CC: Rome, 2008; Vol. 2, pp 651–659.
71. ISO. ISO 4628-6: 2011. Paints and Varnishes — Evaluation of Degradation of Coatings — Designation of Quantity and Size of Defects, and of Intensity of Uniform Changes in Appearance — Part 6: Assessment of Degree of Chalking by Tape Method, 2011.
72. Giordano, A.; Cremonesi, P. Gel rigidi polisaccaridici per il trattamento dei manufatti artistici; Il Prato, 2019.
73. Giordano, A.; Cremonesi, P. New Methods of Applying Rigid Agar Gels: From Tiny to Large-Scale Surface Areas. *Studies in Conservation*, **2021**, *66* (8), 437–448. https://doi.org/10.1080/00393630.2020.1848272.
74. Giordano, A.; Cremonesi, P. Gel rigidi polisaccaridici per il trattamento dei manufatti artistici; Il Prato, 2019.
75. Keynan, D.; Hughes, A. Testing the Waters: New Technical Applications for the Cleaning of Acrylic Paint Films and Paper Supports. **2013**, 9.
76. Stavroudis, C.; Doherty, T. The Modular Cleaning Program in Practice: Application to Acrylic Paintings. In *Proceedings from the Cleaning 2010 International Conference*; Citeseer: Universidad Politecnica de Valencia and Museum Conservation Institute, 2013; pp 139–145.

77. Stoveland, L. P. Soiling Removal from Painted Mock-Ups. Evaluation of Novel Surface Cleaning Methods on Oil Paint and Chalk-Glue Ground in the Context of the Unvarnished Aula Paitnings by Edvard Munch. PhD, University of Oslo: Oslo, 2021.
78. Stavroudis, C. Gels: Evolution in Practice. In *Gels in the conservation of art*; Angelova, L. V., Ormsby, B., Townsend, J., Eds.; Archetype Publications: London, 2017; pp 209–227.
79. Charola, A. E.; Wachowiak, M.; Webb, E. K.; Grissom, C. A.; Chong, W.; Szczepanowska, H.; DePriest, P. Developing a Methodology to Evaluate the Effectiveness of a Biocide. *New York*, **2012**, 10.
80. Doane, D. P.; Seward, L. E. Measuring Skewness: A Forgotten Statistic? *Journal of Statistics Education*, **2011**, *19* (2), null. https://doi.org/10.1080/10691898.2011.11889611.
81. Mills, J. S.; Smith, P. *Cleaning, Retouching and Coating: Technology and Practice for Easel Paintings and Polychrome Sculpture*; International Institute for Conservation of Historic and Artistic Works, 1990.
82. Szczepanowska, H. M. Conservation of Cultural Heritage: Key Principles and Approaches; Routledge, 2013.
83. *Issues in Contemporary Oil Paint*; van den Berg, K. J., Burnstock, A., de Keijzer, M., Krueger, J., Learner, T., Tagle, de, A., Heydenreich, G., Eds.; Springer International Publishing: Cham, 2014. https://doi.org/10.1007/978-3-319-10100-2.
84. *Conservation of Easel Paintings*, 2nd edition.; Stoner, J. H., Rushfield, R. A., Eds.; Routledge series in conservation and museology; Routledge: New York, 2021.
85. Quabeck, N. Reframing the Notion of "The Artist's Intent:" A Study of Caring for Thomas Hirschhorn's Intensif-Station (2010). *Journal of the American Institute for Conservation*, **2021**, *60* (2–3), 77–91. https://doi.org/10.1080/01971360.2020.1826151.
86. Haralick, R. M.; Shanmugam, K.; Dinstein, I. Textural Features for Image Classification. *IEEE Transactions on Systems, Man, and Cybernetics*, **1973**, *SMC-3* (6), 610–621. https://doi.org/10.1109/TSMC.1973.4309314.
87. Murata, S.; Herman, P.; Lakowicz, J. R. Texture Analysis of Fluorescence Lifetime Images of AT- and GC-Rich Regions in Nuclei. *J Histochem Cytochem*, **2001**, *49* (11), 1443–1451. https://doi.org/10.1177/002215540104901112.
88. Cabrera, J. E. GLCM Texture Analyzer, 2006. https://imagej.nih.gov/ij/plugins/texture.html (accessed Nov 11, 2022).
89. Haralick, R. M.; Shanmugam, K.; Dinstein, I. Textural Features for Image Classification. *IEEE Transactions on Systems, Man, and Cybernetics*, **1973**, *SMC-3* (6), 610–621. https://doi.org/10.1109/TSMC.1973.4309314.
90. Albregtsen, F. Statistical Texture Measures Computed from Gray Level Coocurrence Matrices, 2008.
91. Rosi, F.; Harig, R.; Miliani, C.; Braun, R.; Sali, D.; Daveri, A.; Brunetti, B. G.; Sgamellotti, A. Mid-Infrared Hyperspectral Imaging of Painting Materials; Pezzati, L., Targowski, P., Eds.; Munich, Germany, 2013; p 87900Q. https://doi.org/10.1117/12.2020477.
92. Rosi, F.; Miliani, C.; Braun, R.; Harig, R.; Sali, D.; Brunetti, B. G.; Sgamellotti, A. Noninvasive Analysis of Paintings by Mid-Infrared Hyperspectral Imaging. *Angew. Chem. Int. Ed.*, **2013**, *52* (20), 5258–5261. https://doi.org/10.1002/anie.201209929.
93. Sandak, J.; Sandak, A.; Legan, L.; Retko, K.; Kavčič, M.; Kosel, J.; Poohphajai, F.; Diaz, R. H.; Ponnuchamy, V.; Sajinčič, N.; et al. Nondestructive Evaluation of Heritage Object Coatings with Four Hyperspectral Imaging Systems. *Coatings*, **2021**, *11* (2), 244. https://doi.org/10.3390/coatings11020244.
94. Russo, S.; Brambilla, L.; Thomas, J.-B.; Joseph, E. 2D Chemical Imaging for the Monitoring of the Formation of Metal Soaps on Oil-Painted Copper and Zinc Substrates. In *Metal 2022 Proceedings of the Interim Meeting of the ICOM-CC Metals Working Group September 5-9, 2022 Helsinki, Finland*; ICOM-CC: Helsinki, 2023.
95. Knez, D.; Toulson, B. W.; Chen, A.; Ettenberg, M. H.; Nguyen, H.; Potma, E. O.; Fishman, D. A. Spectral Imaging at High Definition and High Speed in the Mid-Infrared. *Science Advances*, **2022**, *8* (46), eade4247. https://doi.org/10.1126/sciadv.ade4247.
96. Bindokas, V.; Mascalchi, P. ImageJ / Fiji Macro to Automatically Correct White Balance in RGB Images, 2017. https://github.com/pmascalchi/ImageJ_Auto-white-balance-correction (accessed Nov 1, 2022).
97. Image.sc. Auto White Balance of Stack - Image Analysis, 2019. https://forum.image.sc/t/auto-white-balance-of-stack/22439/1 (accessed Nov 1, 2022).
98. Schwartzwald, D. Color Space Converter, 2012. https://imagej.nih.gov/ij/plugins/color-space-converter.html (accessed Nov 1, 2022).
99. Doane, D. P.; Seward, L. E. Measuring Skewness: A Forgotten Statistic? *Journal of Statistics Education*, **2011**, *19* (2), null. https://doi.org/10.1080/10691898.2011.11889611.
100. Pillay, R.; Hardeberg, J. Y.; George, S. Hyperspectral Imaging of Art: Acquisition and Calibration Workflows. *Journal of the American Institute for Conservation*, **2019**, *58* (1–2), 3–15. https://doi.org/10.1080/01971360.2018.1549919.
101. Deborah, H.; George, S.; Hardeberg, J. Y. Spectral-Divergence Based Pigment Discrimination and Mapping: A Case Study on *The Scream* (1893) by Edvard Munch. *Journal of the American Institute for Conservation*, **2019**, *58* (1–2), 90–107. https://doi.org/10.1080/01971360.2018.1560756.

102. Babini, A.; George, S.; Hardeberg, J. Y. Hyperspectral Imaging Workflow for the Acquisition and Analysis of Stained-Glass Panels. In *Optics for Arts, Architecture, and Archaeology VIII*; Groves, R., Liang, H., Eds.; SPIE: Online Only, Germany, 2021; p 51. https://doi.org/10.1117/12.2593735.
103. Babini, A. Hyperspectral Imaging of Stained Glass. PhD, NTNU: Gjøvik, 2023.
104. Grillini, F. Reflectance Imaging Spectroscopy: Fusion of VNIR and SWIR for Cultural Heritage Analysis. PhD, NTNU: Gjøvik, 2023.
105. Cutajar, J. D.; Babini, A.; Deborah, H.; Hardeberg, J. Y.; Joseph, E.; Frøysaker, T. Hyperspectral Imaging Analyses of Cleaning Tests on Edvard Munch's Monumental Aula Paintings. *Studies in Conservation*, **2022**, *67* (sup1), 59–68. https://doi.org/10.1080/00393630.2022.2054617.
106. Vagnini, M.; Miliani, C.; Cartechini, L.; Rocchi, P.; Brunetti, B. G.; Sgamellotti, A. FT-NIR Spectroscopy for Non-Invasive Identification of Natural Polymers and Resins in Easel Paintings. *Anal Bioanal Chem*, **2009**, *395* (7), 2107–2118. https://doi.org/10.1007/s00216-009-3145-6.
107. Hourant, P.; Baeten, V.; Morales, M. T.; Meurens, M.; Aparicio, R. Oil and Fat Classification by Selected Bands of Near-Infrared Spectroscopy. *Appl. Spectrosc., AS*, **2000**, *54* (8), 1168–1174.
108. Duconseille, A.; Andueza, D.; Picard, F.; Santé-Lhoutellier, V.; Astruc, T. Molecular Changes in Gelatin Aging Observed by NIR and Fluorescence Spectroscopy. *Food Hydrocolloids*, **2016**, *61*, 496–503. https://doi.org/10.1016/j.foodhyd.2016.06.007.
109. Eldin, A. B. *Near Infra Red Spectroscopy*; IntechOpen, 2011. https://doi.org/10.5772/24208.
110. Amato, S. R.; Burnstock, A.; Michelin, A. A Preliminary Study on the Differentiation of Linseed and Poppy Oil Using Principal Component Analysis Methods Applied to Fiber Optics Reflectance Spectroscopy and Diffuse Reflectance Imaging Spectroscopy. *Sensors (Basel)*, **2020**, *20* (24), 7125. https://doi.org/10.3390/s20247125.
111. Li, X.; Sun, C.; Zhou, B.; He, Y. Determination of Hemicellulose, Cellulose and Lignin in Moso Bamboo by near Infrared Spectroscopy. *Sci Rep*, **2015**, *5* (1), 17210. https://doi.org/10.1038/srep17210.
112. Catelli, E.; Sciutto, G.; Prati, S.; Chavez Lozano, M. V.; Gatti, L.; Lugli, F.; Silvestrini, S.; Benazzi, S.; Genorini, E.; Mazzeo, R. A New Miniaturised Short-Wave Infrared (SWIR) Spectrometer for on-Site Cultural Heritage Investigations. *Talanta*, **2020**, *218*, 121112. https://doi.org/10.1016/j.talanta.2020.121112.
113. Magnusson, M.; Sigurdsson, J.; Armansson, S. E.; Ulfarsson, M. O.; Deborah, H.; Sveinsson, J. R. Creating RGB Images from Hyperspectral Images Using a Color Matching Function. In *IGARSS 2020 - 2020 IEEE International Geoscience and Remote Sensing Symposium*; 2020; pp 2045–2048. https://doi.org/10.1109/IGARSS39084.2020.9323397.
114. Miller, J. N.; Miller, J. C. *Statistics and Chemometrics for Analytical Chemistry*, 6th ed.; Prentice Hall/Pearson: Harlow, 2018.
115. Luo, M. R.; Cui, G.; Rigg, B. The Development of the CIE 2000 Colour-difference Formula: CIEDE2000. Color Research & Application: Endorsed by Inter-Society Color Council, The Colour Group (Great Britain), Canadian Society for Color, Color Science Association of Japan, Dutch Society for the Study of Color, The Swedish Colour Centre Foundation, Colour Society of Australia, Centre Français de la Couleur, **2001**, 26 (5), 340–350.
116. Habekost, M. Which Color Differencing Equation Should Be Used. *International Circular of Graphic Education and Research*, **2013**, *6*, 20–33.
117. Boronkay, G. Colour Conversion Centre http://ccc.orgfree.com/ (accessed Nov 1, 2022).
118. Williams, J. H. Guide to the Expression of Uncertainty in Measurement (the GUM). *Quantifying Measurement: The tyranny of numbers*, **2016**. https://doi.org/10.1088/978-1-6817-4433-9ch6.
119. Wienand, J.; Wuest, L. Error Propagation Calculator (online tool for any formula) http://www.julianibus.de/ (accessed Nov 1, 2022).
120. Larkin, P. Chapter 3 - Instrumentation and Sampling Methods. In *Infrared and Raman Spectroscopy*; Larkin, P., Ed.; Elsevier: Oxford, 2011; pp 27–54. https://doi.org/10.1016/B978-0-12-386984-5.10003-5.
121. Campbell, W. TN21-03. ATR Crystal Choice and Quest Puck Guide., 2022. https://specac.com/news-atr-spectroscopy-of-carbon-black/ (accessed Jun 13, 2023).
122. Menges, F. Spectragryph - Optical Spectroscopy Software, 2021. http://www.effemm2.de/spectragryph/ (accessed Jun 13, 2023).
123. Botton, G.; Prabhudev, S. Analytical Electron Microscopy. In *Springer Handbook of Microscopy*; Hawkes, P. W., Spence, J. C. H., Eds.; Springer Handbooks; Springer International Publishing: Cham, 2019; pp 345–453. https://doi.org/10.1007/978-3-030-00069-1_7.
124. Erdman, N.; Bell, D. C.; Reichelt, R. Scanning Electron Microscopy. In *Springer Handbook of Microscopy*; Hawkes, P. W., Spence, J. C. H., Eds.; Springer Handbooks; Springer International Publishing: Cham, 2019; pp 229–318. https://doi.org/10.1007/978-3-030-00069-1_5.

 doi:10.20944/preprints202407.0896.v1



125. *Springer Handbook of Microscopy*; Hawkes, P. W., Spence, J. C. H., Eds.; Springer Handbooks; Springer International Publishing: Cham, 2019. https://doi.org/10.1007/978-3-030-00069-1.
126. Morrison, R.; Bagley-Young, A.; Burnstock, A.; van den Berg, K. J.; van Keulen, H. An Investigation of Parameters for the Use of Citrate Solutions for Surface Cleaning Unvarnished Paintings. *Studies in Conservation*, **2007**, *52* (4), 255–270. https://doi.org/10.1179/sic.2007.52.4.255.